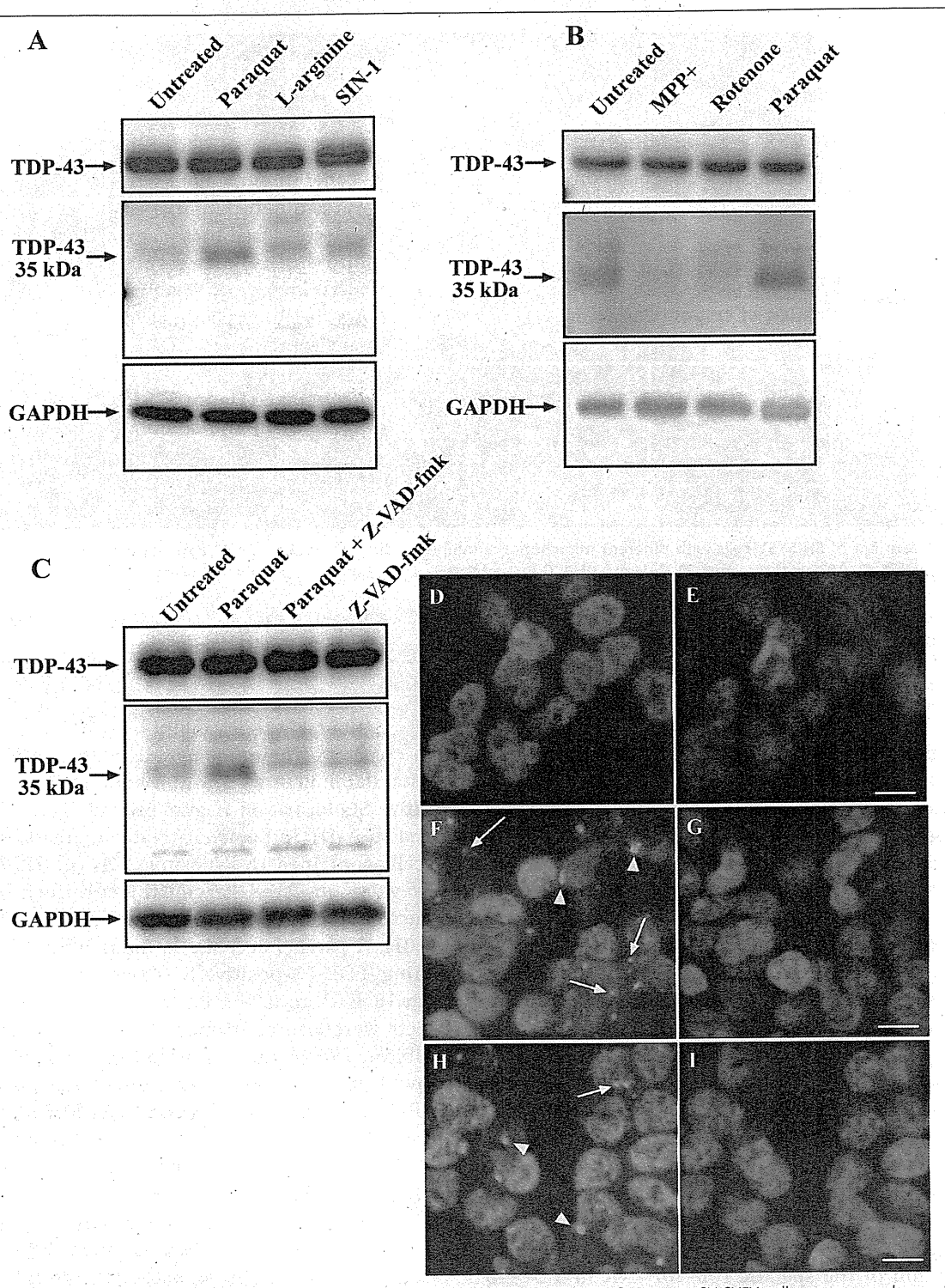

Figure 4 Paraquat treatment induces up-regulation of a caspase-dependent TDP-43 fragment. SH-SY5Y cells were treated overnight with 1 mM paraquat, 1 mM arginine, 100 μM SIN-1 (**A**), or 1 mM paraquat, 2 mM MPP+, 0.075 mM rotenone (**B**) and TDP-43 expression was determined by immunoblot. **C**: Cells were treated overnight with 1 mM paraquat with and without 50 μM Z-VAD-fmk (caspase inhibitor) and TDP-43 expression was determined by immunoblot. Middle panels represent a longer exposure to visualize the 35 kDa band. **D-I:** Cells were treated overnight with paraquat in the absence (**F-G**) and presence (**H-I**) of Z-VAD-fmk and examined for TDP-43-positive SGs. Green = TDP-43, Blue = DAPI. Arrows indicate TDP-43-positive SGs ≤ μm. Arrowheads indicate TDP-43-positive SGs ≥ 1 μm. Bar = 10 μm. Representative images from two-three separate experiments.

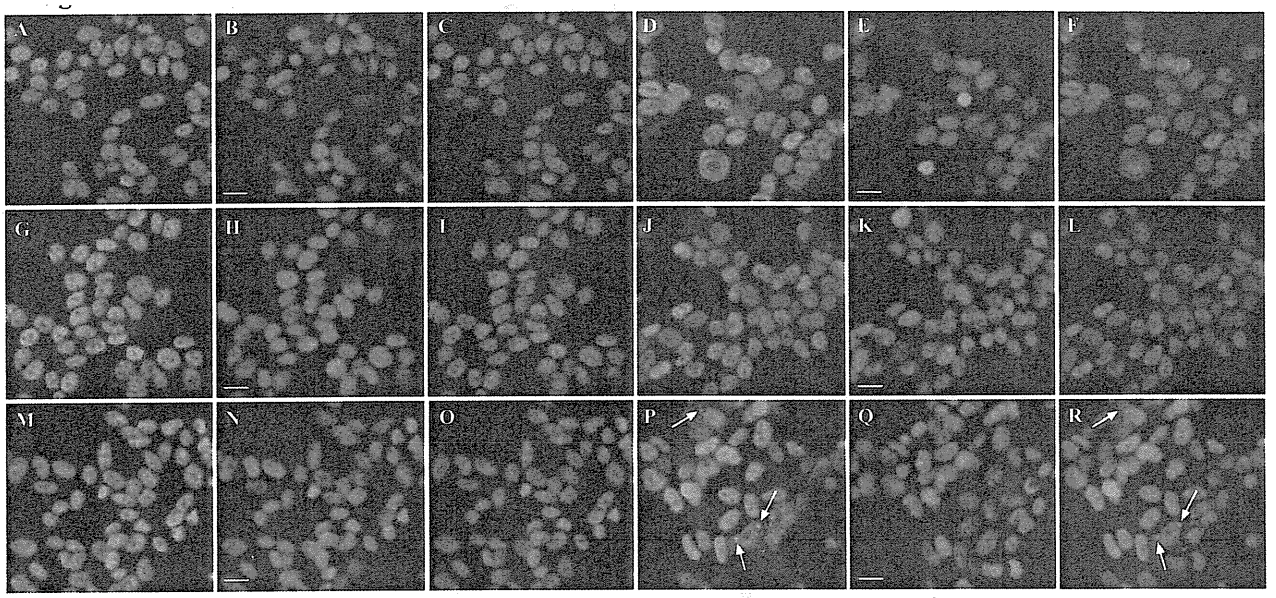

Figure 5 Treatment of SH-SY5Y cells with different mitochondrial inhibitors did not induce TDP-43 aggregation. Cells were treated with vehicle control (**A-C**), 0.075 mM rotenone (**D-F**), 1 mM 3-NP (**G-I**), 2 mM MPP+ (**J-L**), 5 mM sodium azide (**M-O**) or 1 mM paraquat (**P-R**). Cells were analyzed for TDP-43 localization by immunofluorescence. Green = TDP-43, blue = DAPI. C, F, I, L, O and R represent merged images of adjacent TDP-43 and DAPI panels to the left. Arrows indicate TDP-43 SGs in paraquat-treated cells. Bar = 10 μm. Representative images from three separate experiments performed in duplicate or triplicate.

TDP-43-positive SGs, with little effect on the presence of HuR-positive SGs (Figure 6B and 6C-R). This was paralleled by inhibition of JNK phosphorylation (Additional File 4K). The numbers of SGs per cell was used as a more consistent indicator than total number of cells containing SGs. However, in paraquat-treated cultures, the number of cells containing one or more TDP-43-positive SGs was 18 ± 8% of all cells. Co-treatment with SP600125 and paraquat reduced this to 0.22 ± 0.06% of cells ($P < 0.01$). No cells containing SGs were observed in control cultures.

As SP600125 is not entirely specific for JNK, we also tested the effect of BI-78D3, a specific JNK inhibitor on TDP-43 SG formation [40] and found that this induced the same effect as SP600125 (data not shown). This was further supported by the fact that inhibition of another SP600125 target kinase, casein kinase 1 (CK1) with a CK1 inhibitor (D4476), had no effect on TDP-43 or HuR SG formation (Figure 6B). Additional confirmation of the specific role for JNK in TDP-43 accumulation in stress granules was obtained through JNK knockdown. Treatment with combined siRNA against JNK1 and JNK2 significantly reduced JNK expression (Additional File 5A). Subsequent treatment with paraquat resulted in almost no TDP-43-positive stress granules while still inducing HuR-positive stress granules (Additional File 5B-M).

In contrast, inhibition of ERK with PD98059 had a substantial inhibitory effect on both TDP-43 and HuR-positive SG formation (Figure 6B and Figure 7I-L compared to A-D). In paraquat-treated cultures, 27.4 ± 7% of cells contained HuR-positive SGs (no HuR-positive SGs were observed in control cultures). This was reduced to 1.5 ± 0.3% after treatment with PD98059 ($P < 0.01$). A parallel decrease in the number of cells containing TDP-43-positive SGs was observed (reduced from 18 ± 8% to 0.99 ± 0.2% of cells, $P < 0.01$). These effects were also confirmed using the additional ERK inhibitor, U0126 and Raf inhibitor, GW5074 (data not shown). A somewhat weaker effect was observed on TDP-43 and HuR SG formation by SB203580, an inhibitor of p38 (Figure 6B and Figure 7M-P compared to A-D). SB203580 reduced the number of cells containing HuR-positive SGs from 27.4 ± 7% to 12.9 ± 1.7% ($P < 0.01$) and cells containing TDP-43-positive SGs from 18 ± 8 to 7.2 ± 2.1% ($P < 0.01$). Although ERK was activated earlier than p38 by paraquat, the inhibition of HuR and TDP-43-positive SGs by inhibitors of both kinases is consistent with our observations that SGs were not detected until after 8 hr of paraquat exposure (data not shown). This suggests that different kinases may have a role in SG formation over the prolonged exposure to paraquat with JNK controlling TDP-43 association and ERK and p38 affecting TDP-43 and

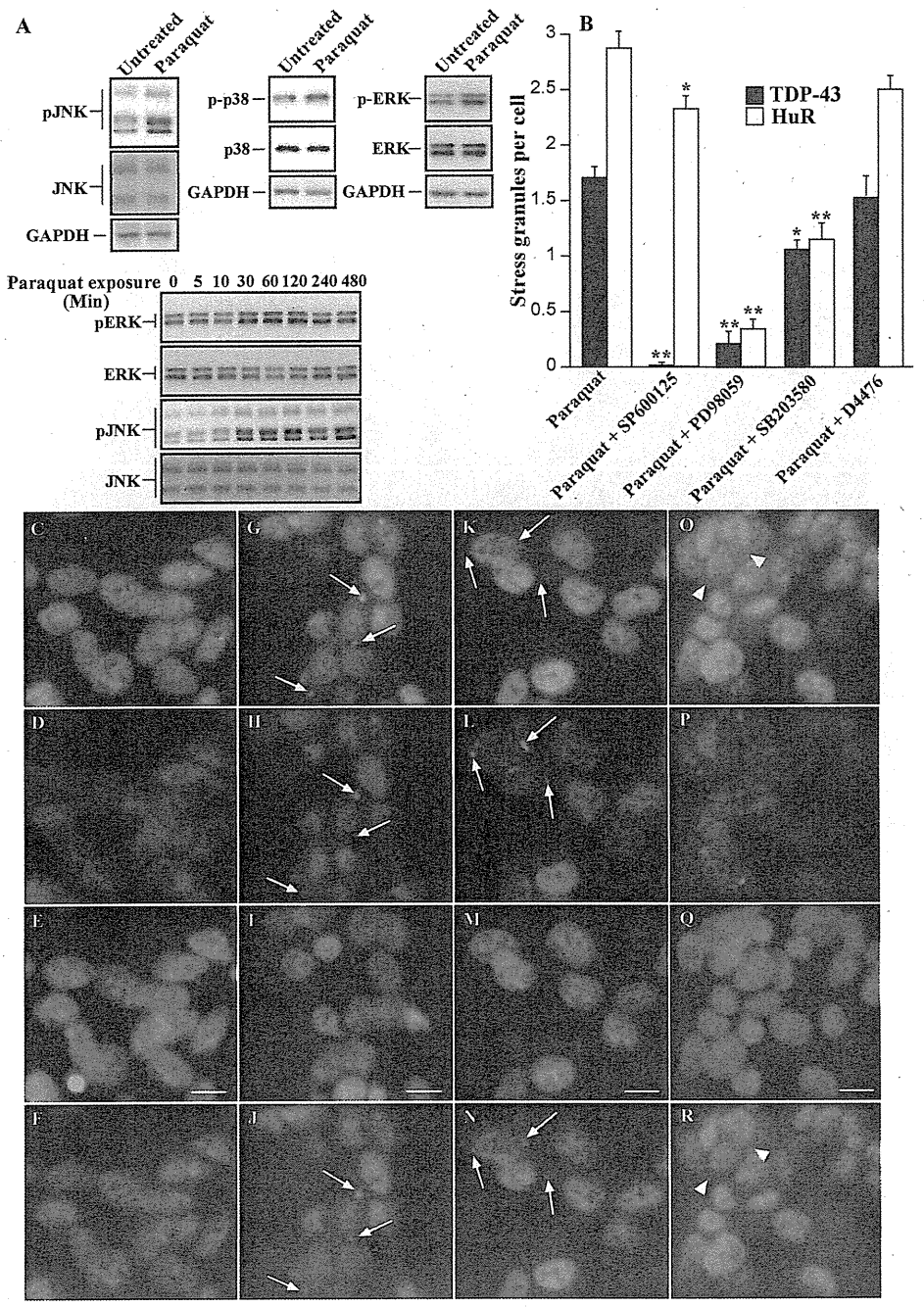

Figure 6 Treatment of SH-SY5Y cells with paraquat induces JNK-dependent accumulation of TDP-43 into SGs. Cells were treated with 1 mM paraquat overnight. Where indicated, cells were co-treated with 10 μM SP600125 (JNK inhibitor), PD98059 (ERK inhibitor), SB203580 (p38 inhibitor) or D4476 (CK1 inhibitor). Cells were examined for phosphorylation of kinases by immunoblot and accumulation of TDP-43 and HuR by immunofluorescence. **A**: Cells were treated with paraquat and examined after overnight incubation for activation of JNK, p38 and ERK. In addition, cells were incubated with paraquat and examined at different time points from 0-480 min (8 hr) for ERK and JNK activation. Lower panels for each image indicate that total kinase expression is unchanged, upper panels indicate changes to phorphorylated forms. **B**: Cells were treated with paraquat in the presence or absence of kinase inhibitors and the number of TDP-43 and HuR SGs was determined. *$p < 0.05$, **$p < 0.01$. n = minimum of 500 cells counted across multiple coverslips and separate experiments for each inhibitor. **C-F**: Untreated, **G-J**: Paraquat treated, **K-N**: Paraquat + SP600125 showing loss of TDP-43 but not HuR SGs, **O-R**: Paraquat + SP600125 showing loss of TDP-43 SGs but not diffuse cytosolic TDP-43. Green = TDP-43, red = HuR, blue = DAPI. Bottom panels indicate merged images of TDP-43 and HuR panels above. Arrows indicate SGs, arrowheads indicate diffuse TDP-43. Bar = 10 μm. Representative images from two-four separate experiments performed in duplicate or triplicate.

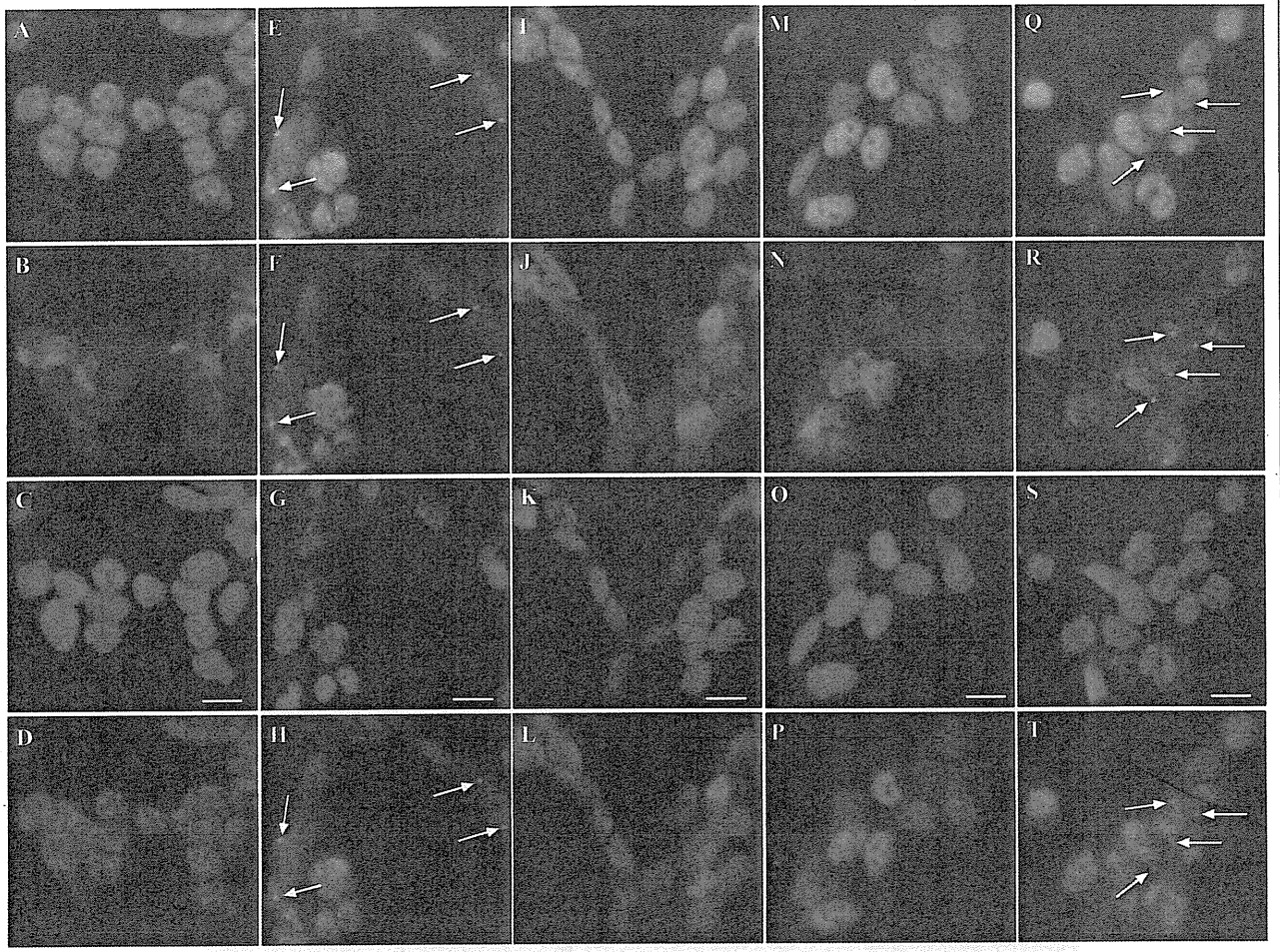

Figure 7 Treatment of SH-SY5Y cells with paraquat induces ERK and p-38-dependent accumulation of TDP-43 and HuR-positive SGs. Cells were treated overnight with 1 mM paraquat in the absence or presence of 10 μM PD98059 (ERK inhibitor), SB203580 (p38 inhibitor) or SP600125 (JNK inhibitor) and immunofluorescence analysis of TDP-43 and HuR was performed. **A-D:** Untreated control, **E-H:** paraquat-treated, **I-L:** paraquat and PD98059, **M-P:** paraquat and SB203580, **Q-T:** paraquat and SB600125. Green = TDP-43, red = HuR, blue = DAPI. Arrows indicate SGs. Bottom panel indicates merged images from TDP-43 and HuR panels above. Bar = 10 μm. Representative images from three separate experiments performed in duplicate or triplicate.

additional SG protein accumulation. This is the first report of JNK and additional kinases controlling TDP-43 localization to SGs. The fact that inhibition of JNK resulted in almost complete abrogation of TDP-43-positive SGs with little effect on HuR localization to SGs indicated that JNK is potentially a key controller of TDP-43 (and possibly other hnRNP) association with SGs rather than simply mediating SG formation *per se*.

As the majority of studies on SGs involve acute (0.5 - 1 hr) treatment with toxic doses of stress inducers such as arsenite, heat shock or osmotic stress, we examined whether a short-term treatment with paraquat induced JNK-controlled TDP-43 SG formation. Interestingly treatment of cells for 1 hr with up to 5 mM paraquat had no effect on HuR or TDP-43 (data not shown), demonstrating that paraquat-mediated SG formation is a longer term process requiring prolonged incubation for TDP-43 to localize to SGs. The data are more consistent with a role for paraquat in prolonged oxidative stress than impairment of mitochondrial function and suggest that paraquat or other chronic inducers of TDP-43 SG formation may provide useful models to mimic the slow progression of disease-associated changes in ALS or FTD.

JNK controls TDP-43 SG association in different cell-types

To determine if the effect of JNK inhibition on TDP-43 localization with SGs in SH-SY5Y cells was specific for this cell-type, we compared this to additional cell-lines treated with paraquat. Treatment of HeLa cells and U87MG glial cells overnight with 1 mM paraquat resulted in TDP-43-positive SGs (Additional File 6). Extensive numbers of TDP-43 SGs were observed in HeLa cells (~28% of cells) while SG positive cells in

U87MG cultures were rare (~2% of cells) (Additional File 6). No paraquat-induced SGs were observed in HEK293 or human fibroblasts (GSM2069) (not shown). Co-treatment of HeLa cultures with paraquat and SP600125, dramatically reduced formation of TDP-43-postive SGs, with only a limited effect on the presence of HuR-positive SGs analogous to SP600125 treatment of SH-SY5Y cells (data not shown). These findings demonstrate that paraquat induces TDP-43-positive SGs in different cell-types and JNK-mediated control of TDP-43 with SGs is not specific for one cell line but appears to be a consistent feature of chronic stress-induced SG formation.

JNK partially controls TDP-43 association with SGs in arsenite stress

We examined whether inhibition of JNK also affected localization of TDP-43 in cells exposed to sodium arsenite, the most commonly used SG inducer. Sodium arsenite is also known to induce JNK activation [41]. Initially, we compared the effect of sodium arsenite on TDP-43 in SH-SY5Y cells at a concentration that induced the same level of toxicity as paraquat did overnight. 50 μM sodium arsenite overnight induced 58% cell viability (compared to 57% cell viability in cells treated with 2 mM paraquat overnight, Additional File 1B). However, this level of toxicity with sodium arsenite did not cause cytosolic TDP-43 SGs. We also examined short term treatment of cells with sodium arsenite (0.5 mM sodium arsenite for 1 hr) and while this induced robust HuR SGs, few cells revealed TDP-43 co-localization. Given the lack of TDP-43 SGs in the sodium arsenite-treated SH-SY5Y cells, we treated HeLa cells with sodium arsenite (0.5 mM 1 hr). This treatment induced widespread TDP-43 and HuR-positive SGs (Figure 8D-F). To determine if JNK activity was responsible for TDP-43 accumulation in sodium arsenite-treated cells, cultures were co-treated with SP600125 and paraquat. Interestingly, we observed a 46% decrease in the number of cells positive for TDP-43 SGs (Figure 8G-I). As with inhibition of paraquat-treated SH-SY5Y cells, SP600125 had little effect on HuR SGs (Figure 8G-I). This partial, but significant, inhibition of TDP-43 localization to SGs by JNK inhibition suggests that JNK has a role in TDP-43-SG interaction during acute sodium arsenite treatment but other factors (e.g. other kinases) are also involved.

JNK inhibition partially modulates aggregation of transfected CTF-TDP-43

Next we investigated whether JNK controls aggregation of transfected CTF-TDP-43 constructs. SH-SY5Y cells were transfected with GFP-tagged vector control, full length TDP-43, CTF-TDP-43 162-414 or CTF-TDP-43 219-414 for 48 hrs. As expected, no aggregates of TDP-43 were observed in cells exposed to vector control (Figure 9A-B) or full length TDP-43 (Figure 9C-D). In contrast, CTF-TDP-43 162-414 or 219-414 induced cytoplasmic aggregates in cells after 48 hr consistent with previous reports [15] (Figure 9E-F and 9I-J). We then treated cultures with SP600125 after 24 hr (to allow transfection to stabilize) and examined the formation of TDP-43 aggregates after a further 24 hr incubation. While treatment with SP600125 did not reduce the number of cells containing aggregated TDP-43, there was a significant decrease in the number of aggregates per cell in cultures transfected with TDP-43 162-414 (Figure 9K-L and 9M) and 219-414 (Figure 9G-H and 9M). ERK inhibition induced a small decrease in number of aggregates but this was not significant. These findings suggested that the aggregation of these CTF-TDP-43 fragments maybe partially affected by JNK. This could be due to a role for basal JNK activity in modulating CTF-TDP-43 aggregation or alternatively, early aggregation of the CTF-TDP-43 fragments could induce cell stress that promotes further CTF-TDP-43 aggregation via JNK activation. This stress may then accelerate aggregation in some cells.

JNK inhibition of TDP-43 SG formation is not due to inhibition of 35 kDa CTF-TDP43 expression

Interestingly, while JNK inhibition blocked TDP-43 incorporation in SGs, it did not have a substantial effect on inhibiting accumulation of diffuse cytosolic TDP-43 or prevent loss of nuclear TDP-43 induced by paraquat treatment (Figure 6C-R). This finding provided further support for the role of JNK in modulating cytosolic TDP-43 incorporation into SGs rather than affecting upstream processes leading to loss of nuclear TDP-43 and accumulation of TDP-43 in the cytosol. Additional support for this was obtained when we examined the effect of JNK inhibition on 35 kDa CTF-TDP-43 accumulation. As shown in Figure 10, co-treatment of cultures with the JNK inhibitor, actually led to an increase in detectable levels of the 35 kDa CTF-TDP-43 rather than inhibit its formation. This is consistent with the data in Figure 4 demonstrating that the formation of TDP-43-positive SGs was not fully prevented by inhibiting 35 kDa CTF-TDP-43 formation using a caspase inhibitor.

JNK inhibition blocks association of hnRNP K and TDP-43 with SGs

In order to obtain an insight into the potential mechanism by which JNK controls TDP-43 association with SGs during chronic stress, we examined co-localization with other hnRNPs. Previous studies have reported that TDP-43 binds to hnRNPs including hnRNP A1 and K

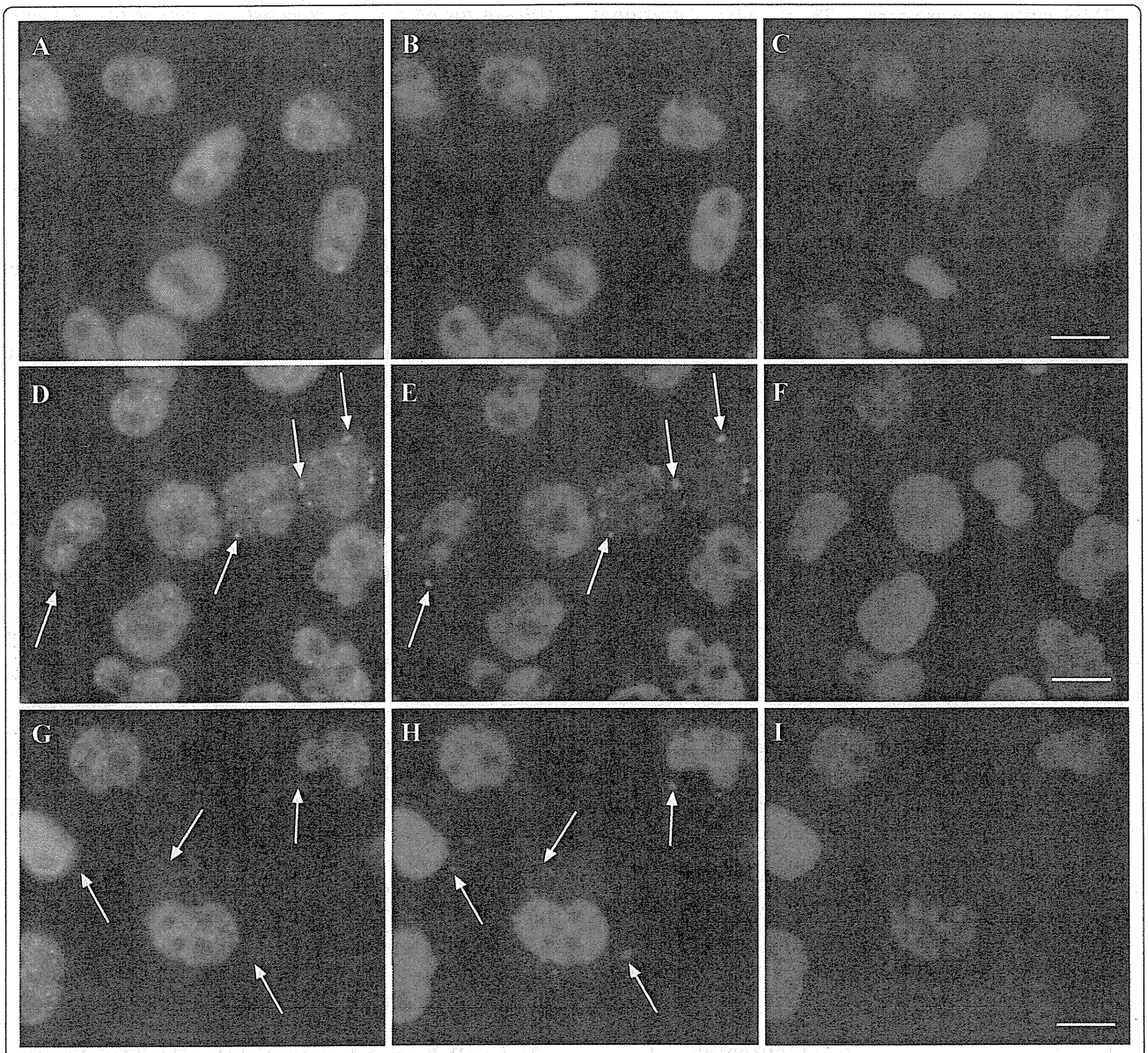

Figure 8 Treatment of HeLa cells with sodium arsenite induces JNK-dependent TDP-43 SGs. HeLa cells were treated for 1 hr with 0.5 mM sodium arsenite and cells were examined for TDP-43 and HuR localization by immunofluorescence. **A-C**: untreated, **D-F**: sodium arsenite-treated, **G-I**: sodium arsenite and SP600125. Green = TDP-43, red = HuR, blue = DAPI. Arrows indicate SGs. Bar = 10 μm. Representative images from three separate experiments performed in duplicate or triplicate.

[25,42] and that stress kinases including JNK can control the cellular localization and SG association of these hnRNPs [31-36]. Analysis of TDP-43 and hnRNP A1 during paraquat stress did not reveal any co-localization within SGs (Figure 10N-Q). In contrast, paraquat-treated cells revealed significant co-localization of hnRNP K and TDP-43 in SGs (Figure 10F-I). Interestingly, JNK inhibition fully blocked both TDP-43 and hnRNP K SG accumulation (Figure 10J-M). As hnRNP K is known to bind to TDP-43, associate with SGs and is phosphorylated by JNK, these findings suggest that modulation of TDP-43 SG association by JNK could be controlled through binding to hnRNP K. However, a comprehensive analysis of hnRNP interactions with JNK and TDP-43 is required to determine if this is the mechanism occurring in paraquat-treated cells and other stress-associated conditions leading to TDP-43 accumulation.

Discussion

Despite considerable research into TDP-43 in the past five years, little is known about the earliest pathological events associated with TDP-43 accumulation in ALS

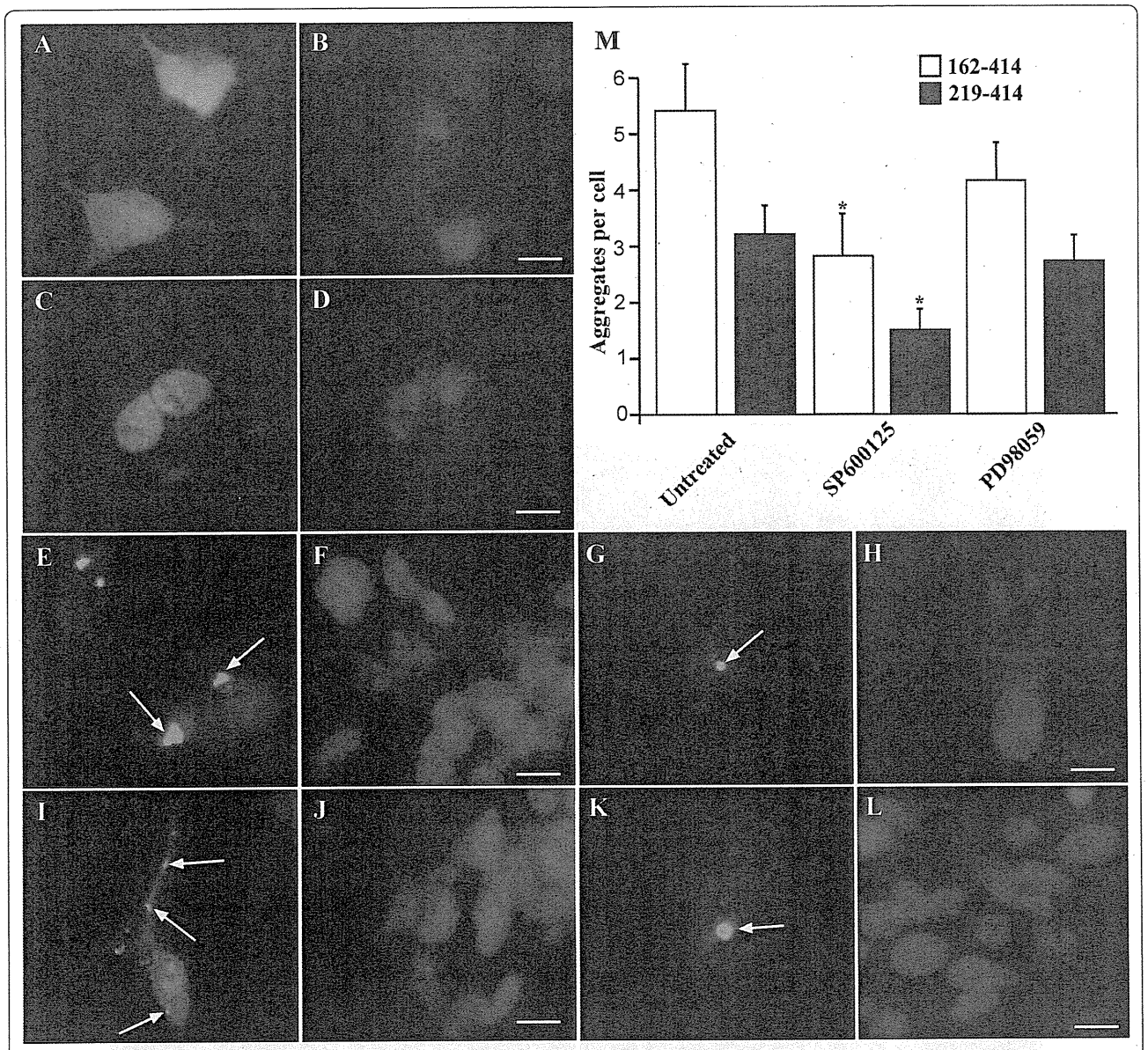

Figure 9 Aggregation of CTF-TDP-43 162-414 and 219-414 in SY5Y cells is partially associated with JNK. SH-SY5Y cells were transfected with GFP-tagged constructs for vector control (**A-B**), full length TDP-43 (**C-D**), CTF-TDP-43 219-414 (**E-H**) or CTF-TDP-43 162-414 (**I-L**). Green = TDP-43-GFP, blue indicates DAPI. Arrows indicate TDP-43 aggregates. Bar = 10 μm. Cells were transfected with CTF-TDP-43 162-414 or 219-414 for 24 hr and co-treated with SP600125 (JNK inhibitor) (**G-H** and **K-L**) or PD98059 (ERK inhibitor) (not shown) for a further 24 hr. The number of TDP-43-GFP aggregates per cell was determined (**M**). **$p < 0.01$. Representative images from two separate experiments performed in triplicate.

and FTD. In this study, we have developed a model of oxidative stress to investigate changes to endogenous TDP-43 processing during cell stresses that reflect the chronic nature of ALS and FTD. We show here that mild stress induced by paraquat, a well-characterized mitochondrial inhibitor and oxidative stress inducer, induced changes to TDP-43 metabolism that closely recapitulated features observed in brain and/or spinal cord of FTD and ALS patients. These changes included clearance of TDP-43 from cell nuclei, accumulation of diffuse TDP-43 in cytosol, aggregation into SGs, ubiquitination of a portion of these SGs and increased expression of the 35 kDa CTF-TDP-43. These are all considered important hallmarks of TDP-43 proteinopathies [6,8]. Importantly, we also found these changes to TDP-43 metabolism in differentiated neurons and additional cell-lines demonstrating that this was not a cell-specific effect. In addition, short term treatment of cells with paraquat (1 hr) had no effect on TDP-43, providing strong support for chronic cell stress as an important

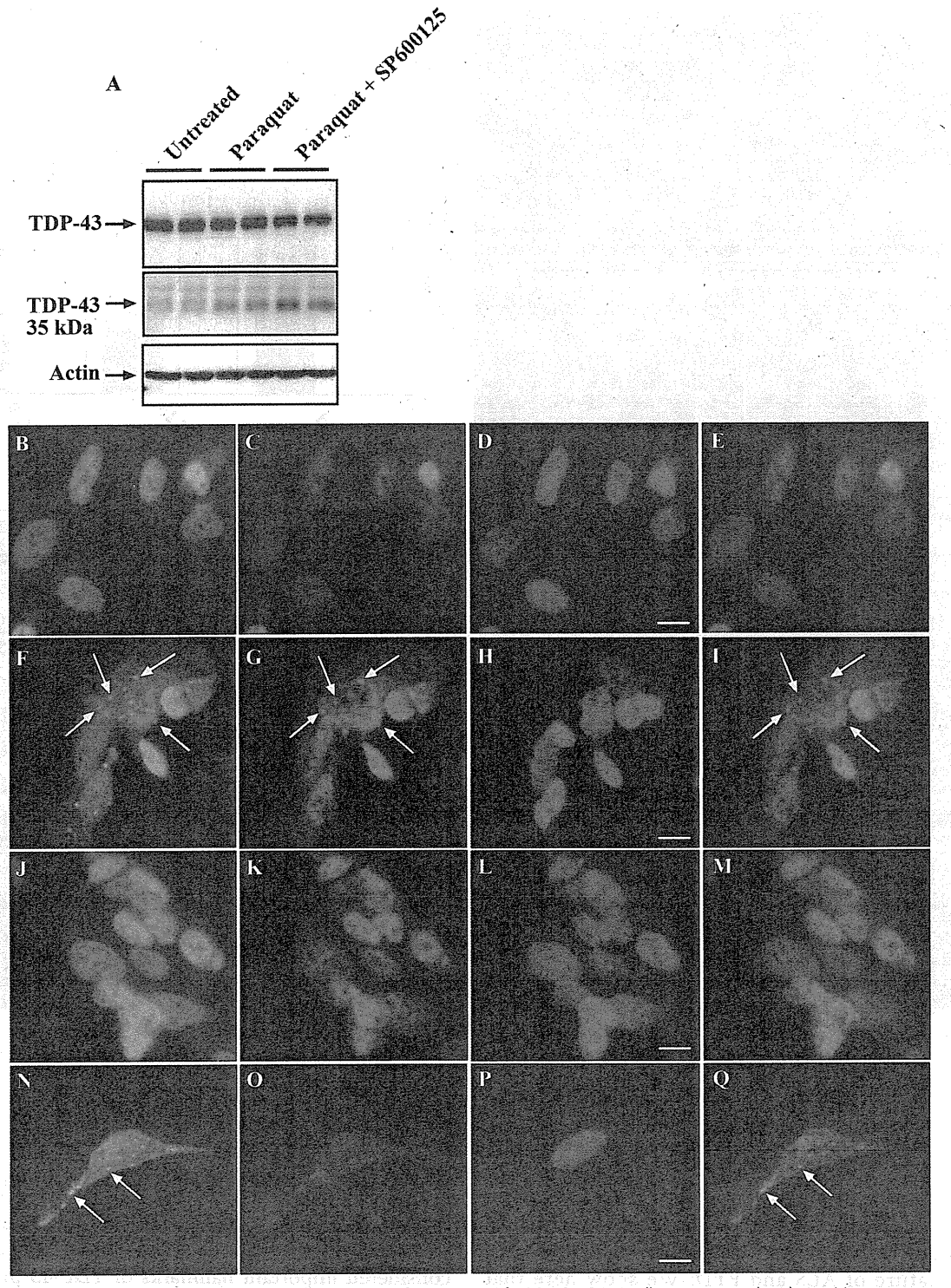

Figure 10 JNK inhibition blocks association of hnRNP K and TDP-43 with SGs. SH-SY5Y cells were treated with 1 mM paraquat overnight in the presence and absence of SP600125. **A**: Cells were immunoblotted for full length TDP-43 and 35 kDa CTF-TDP-43, **B-Q**: Cells were treated with paraquat and SP600125 and examined for TDP-43, hnRNP K or hnRNP A1 by immunofluorescence. **B-E**: untreated, labeled for TDP-43 (green) and hnRNP K (red); **F-I**: paraquat-treated, labeled for TDP-43 (green) and hnRNP K (red); **J-M**: paraquat and SP600125, labeled for TDP-43 (green) and hnRNP K (red); **N-Q** paraquat-treated, labeled for TDP-43 (green) and hnRNP A1 (red). Right-hand panel indicates merged images from TDP-43 and hnRNP panels. Arrows indicate SGs. Bar = 10 μm. Representative images from three separate experiments performed in duplicate or triplicate.

mediator of TDP-43 abnormal processing as observed in ALS and FTD CNS tissues.

The key finding of this study was that cell kinase activity and in particular, JNK activation, modulates TDP-43 localization to SGs. This is the first report of TDP-43 localization controlled by kinase activity. This process is perhaps not surprising as previous reports describe the nuclear-cytoplasmic movement and SG localization of alternative hnRNPs and HuR. Habelhah et. al., have shown that phosphorylation of hnRNP K by ERK can modulate cytoplasmic accumulation [34]. In a separate study they also demonstrated that hnRNP K is phosphorylated by JNK at serine 216 and serine 353 [43]. Moreover, p38 phosphorylates hnRNP A1 inducing SG localization [35,36]. There is also evidence that JNK modulates localization and activity of HuR [44]. Importantly, several studies have shown that HuR and hnRNP A1 and K as well as other hnRNPs directly bind TDP-43 [25,42,45]. Interestingly this is mediated through interaction at the C-terminal region of both proteins. The C-terminal domain of TDP-43 is where the majority of known ALS/FTD disease mutations have been identified [11]. Moreover, there are key JNK phosphorylation consensus sites (Ser/Thr-Pro) within the C-terminal region of hnRNP K and HuR [43]. It is possible that kinase (especially JNK) phosphorylation of hnRNPs modulates interaction with TDP-43, thus mediating SG association. Alternatively, specific phosphorylation of hnRNPs may simply target them to SGs and due to TDP-43 association with these hnRNPs, it becomes localized to SGs where hnRNPs are present. Further support for an hnRNP-TDP-43 association was found in our model where we showed that JNK inhibition blocked localization of both TDP-43 and hnRNP K to SGs. This is particularly interesting as hnRNP K is phosphorylated by JNK [43] and the phosphorylation site lies within the hnRNP C-terminal domain that interacts with TDP-43 in studies on other hnRNPs [42]. Further support for this was shown by the fact that there was no specific localization of hnRNP A1 with paraquat-induced TDP-43 SGs in our study. Interestingly, the only JNK phosphorylation consensus site on hnRNP A1 is in the N-terminal region (Ser7/Pro8) rather than in the C-terminal region that would interact with TDP-43. In addition to these findings, we observed that JNK inhibition did not decrease CTF-TDP-43 generated by paraquat treatment and in fact increased expression. This indicated that JNK is more likely to be controlling localization of cytoplasmic TDP-43 to SGs similar to that reported for other kinases and hnRNPs, rather than modulating the formation of CTF-TDP-43. Whether it is CTF-TDP-43 or full length TDP-43 or both that is aggregating into SGs in this model remains to be seen. Due to the loss of nuclear TDP-43 expression and the fact that CTF-TDP-43 only accounted for approximately 10% of total TDP-43 on Western blots, strongly suggested that the SGs probably contained full length TDP-43 or a mixture of full length and CTF-TDP-43.

There must also be additional factors associated with TDP-43 localization to SGs. JNK activation is not specific for paraquat and in fact, alternative mitochondrial inhibitors used in this study also induce JNK activation [38]. Phosphorylation of JNK is a common downstream effect of oxidative and other cells stresses. The specificity of paraquat to induce JNK-mediated localization of TDP-43 may be related to specific sub-cellular localization of activated JNK or modulation of additional co-factors. Considerable investigation will be required to delineate the specific processes induced by paraquat that leads to JNK-mediated TDP-43 SG accumulation and how these may relate to neurodegenerative diseases such as ALS.

While some recent studies have reported a possible association between TDP-43 and TIA-1 [16,17], these have been demonstrated with transfected cells and no clear evidence of endogenous TDP-43-TIA-1 interaction was identified. Moreover, TIA-1 does not contain JNK consensus sites and there are no reports of JNK control of TIA-1 localization. We believe that the data presented here are more consistent with a potential interaction between TDP-43 and hnRNP K (Figure 11). However, further studies will be required to demonstrate specific interaction in this chronic stress model and to determine if mutation of the C-terminal JNK phosphorylation site on hnRNP K prevents TDP-43 association with SGs. It was also clear from our findings that additional kinases can control TDP-43 and probably a range of hnRNPs during stress. It will take a considerable effort to delineate the role of p38, ERK and additional kinases on TDP-43 accumulation both *in vitro* and *in vivo*.

We also observed partial JNK-mediated control of TDP-43 localization to SGs induced by sodium arsenite, the most common method used for SG induction. The lack of complete inhibition of TDP-43 SG accumulation was possibly related to the fact that sodium arsenite rapidly induces SGs (minutes), while paraquat had no effect on TDP-43 in short-term treatment even at very high doses. This suggests that while sodium arsenite and paraquat induce SGs and both involve JNK, there are different cellular mechanisms involved in short term and longer term SG formation. This is consistent with the previously reported concept that different stresses have diverse affects on SG formation [18]. In this context, we feel that our paraquat-based mild oxidative stress model is an important tool for delineating TDP-43 SG association as it occurs under mild stress conditions expected in chronic neurodegenerative diseases

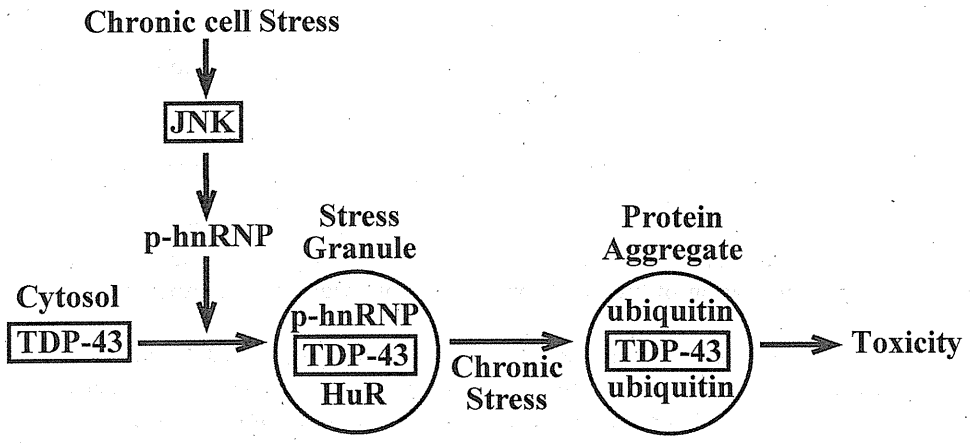

Figure 11 Schematic of proposed stress-mediated TDP-43 accumulation into SGs. Chronic cell stress (eg oxidative stress) induces activation of stress kinases such as JNK. This may phosphorylate hnRNPs such as hnRNP K resulting in phosphoryated forms (p-hnRNP). This could modulate interaction with TDP-43 and association with SGs. Prolonged stress may lead to progression of SGs to protein aggregates containing TDP-43 and subsequent cell toxicity.

and better re-capitulates the features of TDP-43 proteinopatheis than sodium arsenite. It is possible that the latter, (ie acute sodium arsenite exposure) rapidly drives SG formation in cells that are experiencing high levels of toxicity. As shown in Additional File 1B, treatment with 500 μM sodium arsenite overnight results in almost total loss of cell viability as compared to only 15% decrease in viability with 1 mM paraquat overnight.

Whether JNK directly modulates TDP-43 is not known. TDP-43 does not contain known consensus sites for JNK, p38 or ERK. However, it does contain two putative JNK binding domains (RxxxKxxxLxV and KxxRxxxxVxF) at 98-108 and 224-235 respectively. It remains a possibility that JNK binds to TDP-43 and acts as a scaffolding protein affecting SG localization. While no other studies have demonstrated a TDP-43-JNK association, a previous report described a role for a JNK-interacting protein, WDR62 in SG formation [41]. Interestingly, they reported that inhibition of JNK during sodium arsenite treatment increased the number of SGs (in HEK293 cells) but decreased the size of the granules. This is in contrast to our finding in HeLa cells where we found a partial decrease in TDP-43 SG association but no observable changes to HuR SG formation with SP600125. In addition, JNK inhibition did not block SG formation by paraquat as determined by HuR staining but did block TDP-43 and hnRNP K localization. However, these differences are again likely to be due to acute sodium arsenite treatment compared to longer paraquat treatment used here, different cell lines and different markers of SGs eg HuR and TIA-1. Importantly, the findings show that different model systems may give a range of different outcomes and in terms of understanding TDP-43 pathological changes, it will be important to ensure that the model gives an accurate reflection of the disease processes. With that in mind, we are currently investigating TDP-43 metabolism in primary neuronal and glia cell cultures as this may be a more accurate model system to understand TDP-43 SG dynamics.

The role for stress kinases such as JNK and p38 in ALS has been suggested through recent studies. SOD1 ALS models have shown enhanced activity of these kinases as well as modulation of ERK [46-50]. Interestingly, a recent report by Ayala et al. [51] found ERK aggregates in stressed cells and ALS tissues and inhibition of ERK lead to increased TDP-43 aggregation in cultures. While these affects appear to contrast with our own findings, the differences may reflect different intensity and form of stress as well as different cell models and time frame. It will be important to determine the kinetics of ERK and other kinases activation across the disease course in ALS. A single report on JNK activation in ALS patients has described increased activity in astrocytes but not neurons in spinal cord of these patients [52]. We found that paraquat induced TDP-43 aggregation in both neuronal-like and astroglial cell lines in this study. Whether JNK or additional kinases are associated with early changes to TDP-43 accumulation in vivo is not known due to the difficulty of obtaining relevant early disease tissues. It is likely that with the current development of multiple animal models of TDP-43 proteinopathy that re-capitulate human disease neuropathology, we will be able to determine the early events in TDP-43 processing. It is also uncertain what role hnRNPs have in determining TDP-43 aggregation in ALS or FTD. While a large number of hnRNPs have been shown to bind to TDP-43 and many are associated

with SGs, their role in ALS and FTD has not been established. It is important to note, however, that several recent studies have shown that TDP-43 and FUS are associated with SG marker proteins in ALS tissues [17,24].

An important outcome from this study is that kinases may be an important target for therapeutic intervention in ALS and FTD. Should further studies show that kinase activation controls TDP-43 aggregation especially early in disease, it may be possible to inhibit this process with kinase inhibitors. Interestingly, the only approved treatment for slowing ALS disease progression, Riluzole, is known to modulate stress kinase activity [53], and kinase modulators have been discussed previously as possible therapeutic agents for ALS.

Conclusions

In summary, it has been difficult to accurately model endogenous aberrant TDP-43 in cell models. Treatment of cells with sodium arsenite or osmotic stress induces robust TDP-43 containing SGs however, these models have not recapitulated the broad features of TDP-43 mis-metabolism observed in ALS and FTD brain and spinal cord tissues in a manner consistent with transfection of CTF-TDP-43 constructs. The latter however, are likely to be prone to spontaneous aggregation when over-expressed and may not represent an accurate model of the cellular control of TDP-43 processing during chronic stress. Likewise, although studies with mutant TDP-43 constructs can help to understand the disease processes, the majority of ALS and FTD cases are sporadic and probably involve only endogenous, non-mutated TDP-43. Our model has recapitulated a number of features of aberrant endogenous TDP-43 metabolism including loss of nuclear staining, accumulation of diffuse cytoplasmic TDP-43, formation of CTF-TDP-43, aggregation into SGs and ubiqitination of a portion of these SGs indicating the possible transition to irreversible protein aggregates. The aggregation of TDP-43 into SGs is controlled by JNK and SG formation is controlled by additional kinases and these factors are associated with chronic stress. Future studies will be required to fully delineate the mechanism by which kinases control TDP-43 aggregation and whether this is involved in TDP-43 aggregation in vivo. These findings may have important implications for identifying potential therapeutic targets for intervention in ALS and FTD.

Methods

Materials

4',6' Diamino-2-phenylindole dihydrochloride (DAPI) was obtained from Invitrogen (Mount Waverley, Victoria, Australia). (3-(4,5-Dimethylthiazol-2-yl)-2,5-diphenyltetrazolium bromide (MTT), N, N'-dimethyl-4,4'-bipyridinium dichloride (paraquat), rotenone, 1-methyl-4-phenylpyridinium (MPP+), sodium azide, sodium arsenite, 3-nitropropionic acid (3-NP) and 3-Morpholinosyndnomine (SIN-1) were from Sigma Aldrich (Sydney, NSW, Australia) and LDH assay kit was purchased from Roche Diagnostics (Castle Hill, NSW, Australia). SP600125, PD98095, SB203580 were purchased from Merck Biosciences (Melbourne, Victoria, Australia). BI-78D3 and D4476 were purchased from Tocris Bioscience (Ellisville, Melbourne, Victoria, Australia). Z-VAD-fmk was obtained from Promega (Sydney, Australia).

Polyclonal TDP-43 antisera were purchased from Proteintech Group (Chicago, IL, USA). Monoclonal antisera to the phosphorylated form of TDP-43 (ser409/410) were obtained from Cosmo Bio (Tokyo, Japan). Antisera to ubiquitin were from Santa Cruz Biotechnology (Santa Cruz, CA, USA). Monoclonal antisera to hnRNP A1 and hnRNP K were purchased from Abcam (Waterloo, Australia). Monoclonal antisera to HuR were obtained from Invitrogen (Mount Waverley, Victoria, Australia). Antisera to total and phosphorylated forms of p38, ERK and JNK, as well as antibodies to actin and GAPDH were purchased from Cell Signalling Technologies (Arundel, Queensland) or BD Bioscience (North Ryde NSW, Australia).

Methods

Cell Culture

The cell lines used in this study were human neuroblastoma SH-(SY5Y) cell line, human epithelial HeLa cell line, human embryonic kidney cell line (HEK293), human fibroblast cell line (GSM2069) and human astroglial U87MG cell line. Cells were passaged and maintained in DMEM plus 5% FBS (HeLa and HEK293 cells), DMEM/F12 plus 10% FBS (SH-SY5Y and U87MG cells) or BME plus 10% FCS (GSM2069 fibroblasts). To induce differentiation, SY5Y cells were treated with 10 μM retinoic acid for 7 days. Differentiation was confirmed by morphological changes (neurite extension) and up-regulated expression of synaptophysin, tyrosine hydroxylase and VMAT2. All cells were grown in 5% CO_2 at 37°C.

Cell viability and cell lysis assays

Assays for cell viability (MTT) and cell lysis (LDH) were performed as previously described [28].

Exposure of cell to stress

Undifferentiated cells were grown in 24 or 6-well plates or on 12 mm coverslips (for immunofluorescence) for 2-3 days before experiments (~80% confluent). Differentiated SH-SY5Y cells were cultured in the presence of retinoic acid for 7 days before experiments. Inducers of

nitrosative stess (arginine, paraquat and SIN-1) or oxidative stress (rotenone, 3-NP, sodium azide, MPP+, sodium arsenite and paraquat) were prepared in dH_2O and added at indicated concentrations and the medium was briefly mixed by aspiration. Incubations were performed for periods stated in individual experiments. Where indicated, cells were co-treated with kinase inhibitors (SP600125 (JNK), BI-78D3 (JNK), PD98095 & U0126 (ERK), SB203580 &. SB202190 (p38), D4476 (casein kinase 1) from stock solutions prepared at 10 mM in DMSO. Control cultures were treated with vehicle alone. For immunoblotting, cells were harvested into Phosphosafe Extraction Buffer (Merck Biosciences, San Diego, CA, USA) containing protease inhibitor cocktail (Roche Diagnostics) and stored at -80°C until use. For immunofluorescence studies, cells were grown on glass coverslips and fixed by treating with 4% paraformaldehyde for 30 min.

siRNA knockdown of JNK

ON-TARGETPlus human JNK1 siRNA pool, JNK2 siRNA pool and non-targeting siRNA pool (D-001810-10-20, Negative control) were obtained from Dharmacon and resuspended in RNAase free water at 100 μM. Human JNK1 siRNA pool target sequences were 5'-GCCCAGUAAUAUAGUAGUA-3', 5'-GGCAUGGGCUACAAGGAAA-3', 5'-GAAUAGUAUGCGCAGCUUA-3' and 5'-GAUGACGCCUUAUGUAGUG-3'. Human JNK2 siRNA pool target sequences were 5'-UCGUGAACUUGUCCUCUUA-3', 5'-AGCCAACUGUGAGGAAUUA-3', 5'-GGCUGUCGAUGAUAGGUUA-3' and 5'-GAUUGUUUGUGCUGCAUUU-3'. Cells were seeded on coverslips at 5×10^4 cells per cm^2 in Opti-MeM to give 40% confluency on treatment day. Cells were transfected with pooled JNK1 and JNK2 siRNA or Negative control siRNA in Lipfectamine 2000 for 5 hr at room temperature (0.5 μg RNA per well). Media was then replaced with normal SY5Y growth medium overnight before treatment with paraquat (1 mM) overnight. Cells were then collected for Western blot for JNK or fixed for immunofluoresence of TDP-43 and HuR.

Western blot analysis of protein expression and phosphorylation

Cell lysates prepared in Phosphosafe Extraction Buffer at equal protein concentration were mixed with electrophoresis SDS sample buffer and separated on 12% SDS-PAGE Tris-Glycine gels. Proteins were transferred to PVDF membranes and blocked with 4% skim milk solution in PBST before immunoblotting for total or phospho-specific proteins. For detection of total TDP-43, membranes were probed with polyclonal antisera (1:1500) against TDP-43. Secondary antiserum was rabbit-HRP at 1:5,000 dilution. For detection of total and phospho-forms of JNK, ERK and p38, membranes were probed with anti-JNK, anti-ERK or anti-p38 (each at 1:5000) and antisera to phospho-forms of each protein (each at 1:5000). Blots were developed using GE Healthcare ECL Advance Chemiluminescence and imaged on a Fujifilm LAS3000 imager (Berthold, Bundoora, Australia). Expression of GAPDH or actin was determined using antisera at 1:5000 and 1:3000 respectively for protein loading controls where necessary.

Immunofluorescence analysis

SH-SY5Y cells were grown on 12 mm diameter coverslips and treated with stresses as indicated. Cells were fixed with 4% w/v paraformaldehyde in PBS for 30 min and permeabilized with 90% chilled methanol for 5 min. After blocking for 1 hr with 10% normal goat serum, cells were incubated with primary antibody for total TDP-43 (1:1500), ubiquitin (1:150), HuR (1:50), hnRNP A1 (1:200) or hnRNP K (1:200) for 2 hr at room temperature or overnight at 4°C. This was followed by labeling with secondary AlexaFluor or FITC goat anti-mouse or anti-rabbit antisera at 1:500 for 2 hr at room temperature or overnight at 4°C. After washing, the coverslips were incubated with DAPI at 0.5 μg/ml for 5 min and analyzed using a Leica inverted microscope with Zeiss Axiocam digital camera. Images shown are representative of multiple fields and triplicate coverslips per experiment. TDP-43 and HuR-positive stress granules (SGs) were counted in cultures where indicated. A minimum of 500 cells was counted across multiple fields of view (and multiple coverslips) for each treatment. The number of TDP-43 and HuR-positive SGs were counted in these cells. The total number of cells was divided by the total number of SGs to provide a measure of mean SGs per cell. SGs were not observed in untreated cells.

Preparation of TDP-43 plasmids

Plasmid DNA corresponding to GFP-tagged full-length wild-type (WT) TDP-43 (pEGFP-TDP WT), C-terminal fragments of TDP-43, (pEGFP-TDP 162-414 and pEGFP-TDP 219-414) or empty expression vector pEGFP-C1 were prepared as described by Nonaka et al. [15]. Briefly, plasmid DNA was used to transform MAX Efficiency® DH5α™ Competent Cells (Invitrogen, Mount Waverley, Victoria, Australia) as described by the manufacturer. Transformants were grown and colonies were picked based on kanamycin-resistance and grown in liquid culture for subsequent plasmid purification. DNA was purified using the Wizard® *Plus* Midiprep DNA Purification System (Promega Corporation) as per manufacturer's instructions. DNA was quantified and TDP-43 inserts were identified positively by digestion with *BamHI* and *XhoI*.

Transfection and expression of plasmids

SH-SY5Y cells were seeded at 2×10^5 cells per well in 24 well-plates on coverslips. Cells were transfected 24 hr after seeding with the pEGFP-C1 empty vector, pEGFP-TDP WT, pEGFP-TDP 162-414 and pEGFP-TDP 219-414 using Attractene (Qiagen) according to manufacturer's instructions. After 48 hr incubation, cells were fixed with 4% w/v paraformaldehyde in PBS for 30 min. and permeabilized with 90% chilled methanol for 5 min. After washing, the coverslips were incubated with DAPI at 0.5 μg/ml for 5 min and analyzed using a Leica inverted microscope with Zeiss Axiocam digital camera. Expression of TDP-43 was determined by the EGFP-tagged construct. Efficiency of transfection with pEGFP-C1 vector was approximately 20-25%.

Statistical analysis

All data described in graphical representations are mean ± standard error of the mean (SEM) unless stated from a minimum of three experiments. Results were analysed using a two-tailed Student's *t*-test.

Additional material

Additional file 1: SH-SY5Y cell viability after exposure to nitrosative or oxidative stress inducers. SH-SY5Y cells were treated with indicated compounds overnight and cell viability was measured with the MTT assay. **A:** Mild neurotoxicity was induced with all compounds tested. Concentrations were SIN-1, 0.1 mM; arginine, 1 mM; Paraquat, 1 mM and 2 mM; 3-NP, 1 mM; MPP+, 2 mM; sodium azide, 5 mM and rotenone, 0.075 mM. **B:** Comparison of neurotoxicity induced by 1 and 2 mM paraquat or 0.05 mM and 0.5 mM arsenite treatment overnight. *p < 0.05, **p < 0.01. n = three experiments.

Additional file 2: Treatment of SH-SY5Y neurons induces SG formation associated with mild toxicity. Non-differentiated (**A-C**) or differentiated (**D-K**) were treated with 0-2 mM (**A-C**) or 1 mM (**D-K**) paraquat overnight. **A**: Cell viability was determined by MTT assay. **B**: Cell death was determined by LDH assay. **C**: Stress granules (SGs) per cell were determined. *p < 0.05, **p < 0.01. **D-K**: TDP-43 and HuR immunofluorescence was examined in retinoic acid-differentiated neurons after treatment with 1 mM paraquat. Green = TDP-43, Red = HuR, Blue = DAPI. Arrows indicate SGs. Bar = 10 μm. **G** and **K** represent merged images. n = three experiments.

Additional file 3: Paraquat treatment did not induce phosphorylation of TDP-43 in SGs. Cells were treated overnight with 1 mM paraquat and examined for phosphorylated TDP-43 by immunofluorescence. **A-C:** untreated, **D-F:** paraquat treated. Green = HuR, Red = phospho-TDP-43, blue = DAPI. Bar = 10 μm. **G:** Immunoblot for phospho-TDP-43 (p-TDP-43) in paraquat-treated cultures. Representative images from three separate experiments.

Additional file 4: Treatment of SH-SY5Y cells with different mitochondrial inhibitors did not induce HuR SGs. Cells were treated with vehicle control (**A-B**), 2 mM MPP+ (**C-D**), 1 mM 3-NP (**E-F**), 0.075 mM rotenone (**G-H**) or 5 mM sodium azide (**I-J**). Cells were analyzed for HuR localization by immunofluorescence. Red = HuR, blue = DAPI. Bar = 10 μm. **K:** Treatment with 1 mM paraquat (PQ) overnight induced phospho-JNK (pJNK) and this was inhibited by co-treatment with 20 μM SP600125. Representative images from three separate experiments.

Additional file 5: Treatment of SH-SY5Y cells with siRNA to JNK inhibits TDP-43 accumulation in SGs. A: Cells were treated with pooled siRNA against JNK1 and JNK2 or with negative control siRNA and examined for JNK expression. siRNA to JNK significantly reduced expression of JNK1 and JNK2. **B-E:** Untreated control cells. **F-I:** cells treated with negative control siRNA reveal TDP-43 and HuR-positive SGs. **J-M:** Cells treated with siRNA to JNK reveal lack of TDP-43 but not HuR-positive SGs. Green = TDP-43, red = HuR, blue - DAPI. Arrows indicate SGs. Bar = 10 μm. Representative images from two-three separate experiments performed in triplicate.

Additional file 6: Treatment of U87MG astroglial and HeLa epithelial cells with paraquat results in TDP-43 SGs. U87MG (**A-F**) and HeLa (**G-L**) cells were treated overnight with 1 mM paraquat and analyzed for TDP-43 and HuR localization by immunofluorescence. **A-C**: Untreated U87MG cells, **D-F**: paraquat-treated U87MG cells, **G-I**: untreated HeLa cells, **J-L**: paraquat-treated HeLa cells. Green = TDP-43, red = HuR, blue = DAPI. Arrows indicate SGs. Bar = 10 μm. Representative images from three separate experiments performed in duplicate or triplicate.

Abbreviations

ALS: amyotrophic lateral sclerosis; CTF: C-terminal fragment; ERK: extracellular signal-regulated kinase; FTD: frontotemporal dementia; hnRNP: heterogeneous nuclear ribonucleoprotein; JNK: c-JUN N-terminal kinase; SG: stress granule; SOD: superoxide dismutase; TDP-43: TARDP-binding protein 43.

Acknowledgements

This work was supported by funding from the National Health and Medical Research Council of Australia (program grant to ARW and CLM) and the Australian Research Council of Australia (ARC Future Fellowship to Anthony White). Dominic Ng is a recipient of a Faculty of Medicine, Dentistry and Health Sciences, CR Roper Fellowship. Peter Crouch is recipient of a Melbourne Neuroscience Institute Research Fellowship. We would also like to thank the Motor Neuron Disease Research Institute of Australia (Mick Rodger Benalla Research Grant), the Bethlehem Griffiths Research Foundation and the CASS Foundation for their kind support of this work. JM was supported by Motor Neuron Disease Research Institute of Australia (Mick Rodger Benalla Research Grant). SJP was supported by the CASS foundation. LJV was supported by the NHMRC. KAP was supported by The University of Melbourne. JRL, AC, Q-XL and PJC were supported by the NHMRC. KMK was supported by Sigrid Juselius Foundation, Finland. CLM was supported by the Mental Health Research Institute. TN and HM were supported by the Tokyo Institute of Psychiatry.

Author details

[1]Department of Pathology, The University of Melbourne, Victoria, 3010, Australia. [2]Ludwig Institute for Cancer Research, Austin Hospital, Harold Stokes Building, 145-163 Studley Road, Heidelberg, Victoria, 3084, Australia. [3]Bio21 Molecular Science and Biotechnology Institute, The University of Melbourne, Parkville, Victoria, 3052, Australia. [4]Department of Biochemistry and Molecular Biology, The University of Melbourne, Parkville, Victoria, 3052, Australia. [5]The Mental Health Research Institute, Parkville, Victoria, 3052, Australia. [6]Department of Molecular Neurobiology, Tokyo Institute of Psychiatry, Tokyo 156-8585, Japan.

Authors' contributions

JM performed cell culture assays, immunofluorescence studies, immunoblotting and contributed to the preparation of the manuscript. SJP performed cell culture assays, immunofluorescence studies, immunoblotting transfected cells with constructs and contributed to the preparation of the manuscript. LJV prepared TDP-43 CTF constructs. KAP prepared, treated and collected cell cultures for analysis. JRL participated in the study design and coordination, contributed to experimental data collection and helped to draft the manuscript. AC performed cell culture assays, immunofluorescence studies, immunoblotting and contributed to the preparation of the manuscript, Q-XL participated in the study design and coordination, contributed to experimental data collection and helped to draft the manuscript. CLM helped to draft the manuscript. TN generated TDP-43 constructs. MH generated TDP-43 constructs. KMK participated in the study design and coordination, contributed to experimental data collection and helped to draft the manuscript. DCHN and MAB developed molecular tools

for JNK analysis and contributed to the preparation of the manuscript. PJC participated in the study design and coordination, contributed to experimental data collection and helped to draft the manuscript. ARW conceived the study, participated in the study design and coordination, and helped to draft the manuscript. All authors read and approved the final manuscript.

Competing interests
The authors declare that they have no competing interests.

Received: 15 April 2011 Accepted: 8 August 2011
Published: 8 August 2011

References

1. King AE, Dickson TC, Blizzard CA, Woodhouse A, Foster SS, Chung RS, Vickers JC: **Neuron-glia interactions underlie ALS-like axonal cytoskeletal pathology.** *Neurobiol Aging* 2009, **32**:459-469.
2. Barber SC, Shaw PJ: **Oxidative stress in ALS: key role in motor neuron injury and therapeutic target.** *Free Radic Biol Med* 2010, **48**:629-641.
3. Swarup V, Julien JP: **ALS pathogenesis: Recent insights from genetics and mouse models.** *Prog Neuropsychopharmacol Biol Psychiatry* 2010, **35**:363-369.
4. Barmada SJ, Finkbeiner S: **Pathogenic TARDBP mutations in amyotrophic lateral sclerosis and frontotemporal dementia: disease-associated pathways.** *Rev Neurosci* 2010, **21**:251-272.
5. Ferrari R, Kapogiannis D, Huey ED, Momeni P: **FTD and ALS: A Tale of Two Diseases.** *Curr Alzheimer Res* 2011, **8**:273-294.
6. Neumann M, Sampathu DM, Kwong LK, Truax AC, Micsenyi MC, Chou TT, Bruce J, Schuck T, Grossman M, Clark CM, McCluskey LF, Miller BL, Masliah E, Mackenzie IR, Feldman H, Feiden W, Kretzschmar HA, Trojanowski JQ, Lee VM: **Ubiquitinated TDP-43 in frontotemporal lobar degeneration and amyotrophic lateral sclerosis.** *Science* 2006, **314**:130-133.
7. Arai T, Hasegawa M, Akiyama H, Ikeda K, Nonaka T, Mori H, Mann D, Tsuchiya K, Yoshida M, Hashizume Y, Oda T: **TDP-43 is a component of ubiquitin-positive tau-negative inclusions in frontotemporal lobar degeneration and amyotrophic lateral sclerosis.** *Biochem Biophys Res Commun* 2006, **351**:602-611.
8. Chen-Plotkin AS, Lee VM, Trojanowski JQ: **TAR DNA-binding protein 43 in neurodegenerative disease.** *Nat Rev Neurol* 2010, **6**:211-220.
9. Banks GT, Kuta A, Isaacs AM, Fisher EM: **TDP-43 is a culprit in human neurodegeneration, and not just an innocent bystander.** *Mamm Genome* 2008, **19**:299-305.
10. Mackenzie IR, Rademakers R, Neumann M: **TDP-43 and FUS in amyotrophic lateral sclerosis and frontotemporal dementia.** *Lancet Neurol* 2010, **9**:995-1007.
11. Warraich ST, Yang S, Nicholson GA, Blair IP: **TDP-43: a DNA and RNA binding protein with roles in neurodegenerative diseases.** *Int J Biochem Cell Biol* 2010, **42**:1606-169.
12. Nishimura AL, Zupunski V, Troakes C, Kathe C, Fratta P, Howell M, Gallo JM, Hortobagyi T, Shaw CE, Rogelj B: **Nuclear import impairment causes cytoplasmic trans-activation response DNA-binding protein accumulation and is associated with frontotemporal lobar degeneration.** *Brain* 2010, **133**:1763-1771.
13. Igaz LM, Kwong LK, Chen-Plotkin A, Winton MJ, Unger TL, Xu Y, Neumann M, Trojanowski JQ, Lee VM: **Expression of TDP-43 C-terminal Fragments in Vitro Recapitulates Pathological Features of TDP-43 Proteinopathies.** *J Biol Chem* 2009, **284**:8516-24.
14. Zhang YJ, Xu YF, Cook C, Gendron TF, Roettges P, Link CD, Lin WL, Tong J, Castanedes-Casey M, Ash P, Gass J, Rangachari V, Buratti E, Baralle F, Golde TE, Dickson DW, Petrucelli L: **Aberrant cleavage of TDP-43 enhances aggregation and cellular toxicity.** *Proc Natl Acad Sci USA* 2009, **106**:7607-12.
15. Nonaka T, Kametani F, Arai T, Akiyama H, Hasegawa M: **Truncation and pathogenic mutations facilitate the formation of intracellular aggregates of TDP-43.** *Hum Mol Genet* 2009, **18**:3353-3364.
16. McDonald KK, Aulas A, Destroismaisons L, Pickles S, Beleac E, Camu W, Rouleau GA, Vande Velde C: **TAR DNA-binding protein 43 (TDP-43) regulates stress granule dynamics via differential regulation of G3BP and TIA-1.** *Hum Mol Genet* 2011, **20**:1400-1410.
17. Liu-Yesucevitz L, Bilgutay A, Zhang YJ, Vanderwyde T, Citro A, Mehta T, Zaarur N, McKee A, Bowser R, Sherman M, Petrucelli L, Wolozin B: **Tar DNA binding protein-43 (TDP-43) associates with stress granules: analysis of cultured cells and pathological brain tissue.** *PLoS One* 2010, **5**:e13250.
18. Buchan JR, Parker R: **Eukaryotic stress granules: the ins and outs of translation.** *Mol Cell* 2009, **36**:932-941.
19. Colombrita C, Zennaro E, Fallini C, Weber M, Sommacal A, Buratti E, Silani V, Ratti A: **TDP-43 is recruited to stress granules in conditions of oxidative insult.** *J Neurochem* 2009, **111**:1051-1061.
20. Dewey CM, Cenik B, Sephton CF, Dries DR, Mayer Pr, Good SK, Johnson BA, Herz J, Yu G: **TDP-43 is directed to stress granules by sorbitol, a novel physiological osmotic and oxidative stressor.** *Mol Cell Biol* 2010, **31**:1098-108.
21. Moisse K, Volkening K, Leystra-Lantz C, Welch I, Hill T, Strong MJ: **Divergent patterns of cytosolic TDP-43 and neuronal progranulin expression following axotomy: implications for TDP-43 in the physiological response to neuronal injury.** *Brain Res* 2009, **1249**:202-211.
22. Volkening K, Leystra-Lantz C, Yang W, Jaffee H, Strong MJ: **Tar DNA binding protein of 43 kDa (TDP-43), 14-3-3 proteins and copper/zinc superoxide dismutase (SOD1) interact to modulate NFL mRNA stability. Implications for altered RNA processing in amyotrophic lateral sclerosis (ALS).** *Brain Res* 2009, **1305**:168-182.
23. Ito D, Seki M, Tsunoda Y, Uchiyama H, Suzuki N: **Nuclear transport impairment of amyotrophic lateral sclerosis-linked mutations in FUS/TLS.** *Ann Neurol* 2011, **69**:152-162.
24. Dormann D, Rodde R, Edbauer D, Bentmann E, Fischer I, Hruscha A, Than ME, Mackenzie IR, Capell A, Schmid B, Neumann M, Haass C: **ALS-associated fused in sarcoma (FUS) mutations disrupt Transportin-mediated nuclear import.** *EMBO J* 2010, **29**:2841-2857.
25. Freibaum BD, Chitta RK, High AA, Taylor JP: **Global analysis of TDP-43 interacting proteins reveals strong association with RNA splicing and translation machinery.** *J Proteome Res* 2010, **9**:1104-1120.
26. Barber SC, Mead RJ, Shaw PJ: **Oxidative stress in ALS: A mechanism of neurodegeneration and a therapeutic target.** *Biochim Biophys Acta* 2006, **1762**:1051-1067.
27. Nonaka T, Arai T, Buratti E, Baralle FE, Akiyama H, Hasegawa M: **Phosphorylated and ubiquitinated TDP-43 pathological inclusions in ALS and FTLD-U are recapitulated in SH-SY5Y cells.** *FEBS Lett* 2009, **583**:394-400.
28. Caragounis A, Price KA, Soon CP, Filiz G, Masters CL, Li QX, Crouch PJ, White AR: **Zinc induces depletion and aggregation of endogenous TDP-43.** *Free Radic Biol Med* 2010, **48**:1152-1161.
29. Dormann D, Capell A, Carlson AM, Shankaran SS, Rodde R, Neumann M, Kremmer E, Matsuwaki T, Yamanouchi K, Nishihara M, Haass C: **Proteolytic processing of TAR DNA binding protein-43 by caspases produces C-terminal fragments with disease defining properties independent of progranulin.** *J Neurochem* 2009, **110**:1082-1094.
30. Nishimoto Y, Ito D, Yagi T, Nihei Y, Tsunoda Y, Suzuki N: **Characterization of alternative isoforms and inclusion body of the TAR DNA-binding protein-43.** *J Biol Chem* 2010, **285**:608-619.
31. Chang JW, Koike T, Iwashima M: **hnRNP-K is a nuclear target of TCR-activated ERK and required for T-cell late activation.** *Int Immunol* 2009, **21**:1351-1361.
32. Zhou R, Shanas R, Nelson MA, Bhattacharyya A, Shi J: **Increased expression of the heterogeneous nuclear ribonucleoprotein K in pancreatic cancer and its association with the mutant p53.** *Int J Cancer* 2010, **126**:395-404.
33. Buxade M, Parra JL, Rousseau S, Shpiro N, Marquez R, Morrice N, Bain J, Espel E, Proud CG: **The Mnks are novel components in the control of TNF alpha biosynthesis and phosphorylate and regulate hnRNP A1.** *Immunity* 2005, **23**:177-189.
34. Habelhah H, Shah K, Huang L, Ostareck-Lederer A, Burlingame AL, Shokat KM, Hentze MW, Ronai Z: **ERK phosphorylation drives cytoplasmic accumulation of hnRNP-K and inhibition of mRNA translation.** *Nat Cell Biol* 2001, **3**:325-330.
35. Shimada N, Rios I, Moran H, Sayers B, Hubbard K: **p38 MAP kinase-dependent regulation of the expression level and subcellular distribution of heterogeneous nuclear ribonucleoprotein A1 and its involvement in cellular senescence in normal human fibroblasts.** *RNA Biol* 2009, **6**:293-304.
36. Guil S, Long JC, Caceres JF: **hnRNP A1 relocalization to the stress granules reflects a role in the stress response.** *Mol Cell Biol* 2006, **26**:5744-5758.
37. Bogoyevitch MA, Ngoei KR, Zhao TT, Yeap YY, Ng DC: **c-Jun N-terminal kinase (JNK) signaling: recent advances and challenges.** *Biochim Biophys Acta* 2010, **1804**:463-745.

38. Yang W, Tiffany-Castiglioni E, Koh HC, Son IH: **Paraquat activates the IRE1/ASK1/JNK cascade associated with apoptosis in human neuroblastoma SH-SY5Y cells.** *Toxicol Lett* 2009, **191**:203-210.
39. Choi WS, Abel G, Klintworth H, Flavell RA, Xia Z: **JNK3 mediates paraquat- and rotenone-induced dopaminergic neuron death.** *J Neuropathol Exp Neurol* 2010, **69**:511-520.
40. Stebbins JL, De SK, Machleidt T, Becattini B, Vazquez J, Kuntzen C, Chen LH, Cellitti JF, Riel-Mehan M, Emdadi A, Solinas G, Karin M, Pellecchia M: **Identification of a new JNK inhibitor targeting the JNK-JIP interaction site.** *Proc Natl Acad Sci USA* 2008, **105**:16809-16813.
41. Wasserman T, Katsenelson K, Daniliuc S, Hasin T, Choder M, Aronheim A: **A novel c-Jun N-terminal kinase (JNK)-binding protein WDR62 is recruited to stress granules and mediates a nonclassical JNK activation.** *Mol Biol Cell* 2010, **21**:117-130.
42. Buratti E, Brindisi A, Giombi M, Tisminetzky S, Ayala YM, Baralle FE: **TDP-43 binds heterogeneous nuclear ribonucleoprotein A/B through its C-terminal tail: an important region for the inhibition of cystic fibrosis transmembrane conductance regulator exon 9 splicing.** *J Biol Chem* 2005, **280**:37572-37584.
43. Habelhah H, Shah K, Huang L, Burlingame AL, Shokat KM, Ronai Z: **Identification of new JNK substrate using ATP pocket mutant JNK and a corresponding ATP analogue.** *J Biol Chem* 2001, **276**:18090-18095.
44. Hostetter C, Licata LA, Witkiewicz A, Costantino CL, Yeo CJ, Brody JR, Keen JC: **Cytoplasmic accumulation of the RNA binding protein HuR is central to tamoxifen resistance in estrogen receptor positive breast cancer cells.** *Cancer Biol Ther* 2008, **7**:1496-1506.
45. D'Ambrogio A, Buratti E, Stuani C, Guarnaccia C, Romano M, Ayala YM, Baralle FE: **Functional mapping of the interaction between TDP-43 and hnRNP A2 in vivo.** *Nucleic Acids Res* 2009, **37**:4116-4126.
46. Perlson E, Jeong GB, Ross JL, Dixit R, Wallace KE, Kalb RG, Holzbaur EL: **A switch in retrograde signaling from survival to stress in rapid-onset neurodegeneration.** *J Neurosci* 2009, **29**:9903-9917.
47. Zhu X, Perry G, Smith MA: **Amyotrophic lateral sclerosis: a novel hypothesis involving a gained 'loss of function' in the JNK/SAPK pathway.** *Redox Rep* 2003, **8**:129-133.
48. Veglianese P, Lo Coco D, Bao Cutrona M, Magnoni R, Pennacchini D, Pozzi B, Gowing G, Julien JP, Tortarolo M, Bendotti C: **Activation of the p38MAPK cascade is associated with upregulation of TNF alpha receptors in the spinal motor neurons of mouse models of familial ALS.** *Mol Cell Neurosci* 2006, **31**:218-231.
49. Kim EK, Choi EJ: **Pathological roles of MAPK signaling pathways in human diseases.** *Biochim Biophys Acta* 2010, **1802**:396-405.
50. Atzori C, Ghetti B, Piva R, Srinivasan AN, Zolo P, Delisle MB, Mirra SS, Migheli A: **Activation of the JNK/p38 pathway occurs in diseases characterized by tau protein pathology and is related to tau phosphorylation but not to apoptosis.** *J Neuropathol Exp Neurol* 2001, **60**:1190-1197.
51. Ayala V, Granado-Serrano A, Cacabelos D, Naudí A, Ilieva V, Boada J, Caraballo-Miralles V, Lladó J, Ferrer I, Pamplona R, Portero-Otin M: **Cell stress induces TDP-43 pathological changes associated with ERK1/2 dysfunction: implications in ALS.** *Acta Neuropathol* 2011.
52. Migheli A, Piva R, Atzori C, Troost D, Schiffer D: **c-Jun, JNK/SAPK kinases and transcription factor NF-kappa B are selectively activated in astrocytes, but not motor neurons, in amyotrophic lateral sclerosis.** *J Neuropathol Exp Neurol* 1997, **56**:1314-1322.
53. Stevenson A, Yates DM, Manser C, De Vos KJ, Vagnoni A, Leigh PN, McLoughlin DM, Miller CC: **Riluzole protects against glutamate-induced slowing of neurofilament axonal transport.** *Neurosci Lett* 2009, **454**:161-164.

doi:10.1186/1750-1326-6-57
Cite this article as: Meyerowitz *et al.*: C-Jun N-terminal kinase controls TDP-43 accumulation in stress granules induced by oxidative stress. *Molecular Neurodegeneration* 2011 **6**:57.

JBC Papers in Press. Published on March 5, 2012 as Manuscript M111.325456
The latest version is at http://www.jbc.org/cgi/doi/10.1074/jbc.M111.325456

Phenolic Compounds Prevent Amyloid β-Protein Oligomerization and Synaptic Dysfunction by Site Specific Binding*

Kenjiro Ono[1], Lei Li[2], Yusaku Takamura[3], Yuji Yoshiike[4], Lijun Zhu[2], Fang Han[2], Xian Mao[2], Tokuhei Ikeda[1], Jun-ichi Takasaki[1], Hisao Nishijo[3], Akihiko Takashima[4], David B. Teplow[5], Michael G. Zagorski[2], and Masahito Yamada[1]

[1]Department of Neurology and Neurobiology and Aging, Kanazawa University Graduate School of Medical Science, Kanazawa 920-8640, Japan, [2]Department of Chemistry, Case Western Reserve University, Cleveland, OH 44106 USA, [3]System Emotional Science, University of Toyama, Toyama 930-0194, Japan, [4]Laboratory for Alzheimer's Disease, Brain Science Institute, Riken, 2-1 Hirosawa, Wako, Saitama 351-0198, Japan and [5]Department of Neurology and Mary S. Easton Center for Alzheimer's Disease Research at UCLA, David Geffen School of Medicine, and Molecular Biology Institute and Brain Research Institute, University of California, Los Angeles, CA 90095 USA

*Running title: Phenolic Compounds Prevent Aβ Oligomerization

*To whom correspondence should be addressed to Michael G. Zagorski, Department of Chemistry, Case Western Reserve University, Cleveland, OH 44106 USA, Tel.: +1- 216-368-3706;Fax: +1- 216-368-3006 E-mail: michael.zagorski@case.edu or Masahito Yamada, Department of Neurology and Neurobiology of Aging, Kanazawa University Graduate School of Medical Science, Kanazawa 920-8640, Japan, Tel.: +81-76-265-2290; Fax: +81-76-234-4253; E-mail: m-yamada@med.kanazawa-u.ac.jp

Key words: amyloid β-protein, Alzheimer's disease, phenolic compounds, oligomer, synaptic toxicity

CAPSULE

Background: Epidemiological evidence suggests that consumption of phenolic compounds reduce the incidence of Alzheimer's disease (AD).

Results: Myricetin and rosmarinic acid reduced cellular and synaptic toxicities by inhibition of amyloid β-protein (Aβ) oligomerization. Myricetin promoted NMR changes of Aβ.

Conclusion: Phenolic compounds are worthy therapeutic candidates for AD.

Significance: Phenolic compounds blocked early assembly processes of Aβ through differently binding.

SUMMARY

Cerebral deposition of amyloid β-protein (Aβ) is an invariant feature of Alzheimer's disease (AD), and epidemiological evidence suggests that moderate consumption of foods enriched with phenolic compounds reduce the incidence of AD. We previously reported that the phenolic compounds myricetin (Myr) and rosmarinic acid (RA) inhibited Aβ aggregation *in vitro* and *in vivo*. To elucidate a mechanistic basis for these results, we analyzed the effects of five phenolic compounds in the Aβ aggregation process and in oligomer-induced synaptic toxicities. We now report that the phenolic compounds blocked Aβ oligomerization, and Myr promoted significant NMR chemical shift changes of monomeric Aβ. Both Myr and RA reduced cellular toxicity and synaptic dysfunction of the Aβ oligomers. These results suggest that Myr and RA may play key roles in blocking the toxicity and early assembly processes associated with Aβ through differently binding.

Alzheimer's disease (AD) has been characterized historically by the accumulation of intraneuronal filaments formed by the microtubule-associated protein tau and of extracellular parenchymal and vascular amyloid deposits largely comprising the amyloid β-protein (Aβ) (1). Continuing investigations of

the pathogenetic relationships among tau, Aβ, and AD suggest that oligomeric forms of Aβ play a seminal role in disease causation (1,2). More recent evidence suggests that low n-order oligomers are especially important (3). Townsend *et al.* found that Aβ trimers fully inhibit long-term potentiation, whereas dimers and tetramers have an intermediate potency (4). Dimers and trimers from the conditioned medium of amyloid precursor protein (APP)-expressing CHO cells have been found to cause progressive loss of synapses in organotypic rat hippocampal slices (5). Aβ oligomers extracted from AD brains disrupt synaptic function, and dimers were the smallest oligomers showing activity (6). Recently, structure–cytotoxicity studies of pure Aβ oligomer populations produced the first determinations of oligomer specific activity (7), in that dimers, trimers, and tetramers all were significantly more toxic than monomers. Importantly, a non-linear dependence of cytotoxicity on oligomer order was observed. Thus, the most efficacious therapeutic agents should perhaps target monomeric Aβ and prevent its assembly into any sized oligomer (3).

Nature itself may have created useful therapeutic agents of AD. The relevance of this finding to AD has come from French and Danish epidemiological studies suggesting that moderate wine drinking may protect against AD (8,9). Investigation of this phenomenon may reveal the answer for wine's protective effects against AD. Classical biochemical fractionation studies have shown that the active components of red wine are phenolic compounds, including resveratrol and the proanthocyanidins (10). Resveratrol was found to lower significantly the levels of secreted and intracellular Aβ produced in a variety of cell lines by increasing proteasome-mediated Aβ degradation (11). Interestingly, a related polyphenolic compound, curcumin (Cur), is found in the common spice curry (12). As with red wine, epidemiologic studies have shown a correlation between curry consumption and decreased AD risk (13). The concordance of results from these different systems emphasizes the potential importance of elucidating the mechanism through which phenolic compounds may alter Aβ aggregation and toxicity.

Initial mechanistic studies have focused on formation of large aggregates, Aβ fibrils (fAβ). Phenolic compounds, such as the wine related polyphenol myricetin (Myr), a major component of curry spice turmeric Cur, its analog rosmarinic acid (RA), nordihydroguaiaretic acid (NDGA), and ferulic acid (FA) inhibit the formation of fAβ as well as dissociate preformed fibrils by preferentially and reversibly binding to these structures (14-16). In cell culture experiments, Myr-treated fAβ were less toxic than intact fAβ (14). Recently, a commercially available grape seed polyphenolic extract, MegaNatural®, was shown to inhibit significantly the aggregation of Aβ into sodium dodecyl sulfate (SDS)-stable high molecular weight (HMW) oligomers (15-20 monomers) using AD model transgenic animals (Tg2576)(17). We showed that the phenolic compounds such as Myr, Cur, and RA prevented the development of AD pathology and reduced HMW oligomers in Tg2576 mice(18).

In the studies reported here, we sought to determine how the phenolic compounds affected Aβ conformational dynamics and the early stages of Aβ assembly. To do so, we analyzed the assembly of the Aβ42 and Aβ40 with five phenolic compounds, Myr, FA, NDGA, Cur, and RA (**Fig. 1**) using several well-established techniques for studying amyloid formation, including photo-induced cross-linking of unmodified proteins (PICUP), atomic force microscopy (AFM), circular dichroism spectroscopy (CD), and nuclear magnetic resonance (NMR). Next, we examined whether the phenolic compounds reduced Aβ assembly-induced cytotoxicity and synaptic dysfunction using 3-[4,5-dimethylthiazol-2-yl]-2,5-diphenyltetrazolium bromide (MTT) assays and electrophysiological assays for long-term potentiation (LTP) and depression (LTD) in hippocampal slices.

EXPERIMENTAL PROCEDURES

Chemicals and reagents - Chemicals were obtained from Sigma-Aldrich Co. (St. Louis, MO) and were of the highest purity available. Water was produced using a Milli-Q system

(Nihon Millipore K.K., Japan).

Proteins and phenolic compounds - Aβ peptides were synthesized, purified, and characterized as described previously (19,20). Briefly, synthesis was performed on an automated peptide synthesizer (Model 433A, Applied Biosystems, CA) using 9-fluorenylmethoxycarbonyl-based methods on pre-loaded Wang resins. Peptides were purified using reverse-phase high-performance liquid chromatography (RP-HPLC). Quantitative amino acid analysis and mass spectrometry yielded the expected compositions and molecular weights, respectively, for each peptide. Purified peptides were stored as lyophilizates at –20°C. [Met(O)^{35}]Aβ42 peptide was purchased from Bachem AG (Bubendorf, Switzerland). To prepare peptides for study, Aβ peptide lyophilizates were dissolved at a nominal concentration of 25 or 50 μM in 10% (v/v) 60 mM NaOH and 90% (v/v) 10 mM phosphate buffer, pH 7.4. After sonication for 1 min, the peptide solution was centrifuged for 10 min at 16,000 x *g*. A stock solution of GST (Sigma-Aldrich, St. Louis, MO) was prepared by dissolving the lyophilizate to a concentration of 250 μM in 60 mM NaOH. Prior to use, aliquots were diluted 10-fold into 10 mM sodium phosphate, pH 7.4. We examined 5-phenolic compounds such as Myr, FA, NDGA, Cur, and RA. They were dissolved in ethanol to a final concentration of 2.5 mM and then diluted with 10 mM phosphate, pH 7.4, to produce concentrations of 5, 10, 25, 50, 100, and 500 μM for CD, PICUP, and AFM, as described previously (19).

CD - CD spectra of Aβ:compound mixtures were acquired immediately after sample preparation or following 2, 3, 5, or 6 days of incubation. CD measurements were made by removing a 200 μl aliquot from the reaction mixture, adding the aliquot to a 1 mm path length CD cuvette (Hellma, Forest Hills, NY), and acquiring spectra in a J-805 spectropolarimeter (JASCO, Japan). The CD cuvettes were maintained on ice prior to introduction into the spectrometer. Following temperature equilibration, spectra were recorded at 22°C from ~190-260 nm at 0.2 nm resolution with a scan rate of 100 nm/min. Ten scans were acquired and averaged for each sample. Raw data were manipulated by smoothing and subtraction of buffer spectra according to the manufacturer's instructions.

Chemical cross-linking and determination of oligomer frequency distributions - Immediately after their preparation, samples were cross-linked using PICUP, as described (21). Briefly, to 18 μl of 50 μM protein solution were added 1 μl of 4 mM tris(2,2'-bipyridyl)dichlororuthenium(II) (Ru(bpy)) and 1 μl of 80 mM ammonium persulfate (APS). The final protein:Ru(bpy):APS molar ratios of Aβ40 or Aβ42 was 1:4:80. The mixture was irradiated for 1 sec with visible light and then the reaction was quenched with 2 μl of 1 M dithiothreitol (DTT) (Invitrogen, CA) in ultrapure water. Determination of the frequency distribution of monomers and oligomers was accomplished using SDS-polyacrylamide gel electrophoresis (SDS-PAGE) and silver staining, as described (21). Briefly, 8 μl of each cross-linked sample was electrophoresed on a 10-20% gradient tricine gel and visualized by silver staining (Invitrogen). Uncross-linked samples were used as controls in each experiment. Densitometry was performed with a luminescent image analyzer (LAS 4000 mini, Fujifilm, Tokyo) and image analysis software (Multi gauge v. 3.2., Fujifilm). The intensity of each band in a lane from the SDS gel was normalized to the sum of the intensities of all the bands in that lane, according to the formula $R_i = I_i \Big/ \sum_{i=1}^{n} I_i$ x 100 (%), where R_i is the normalized intensity of band I and I_i is the intensity of each band i. R_i varies from 0–100. To calculate the oligomers ratio, the sum of oligomers intensities of Aβ40 or Aβ42 with 5, 10, 25, 50, 100, and 500 μM Myr, FA, NDGA, Cur or RA was divided by the sum of oligomers intensities without each compound. The EC_{50} was defined as the concentration of Mel to inhibit αS oligomerization to 50% of the control value. EC_{50} was calculated by sigmoidal curve fitting, using GraphPad Prism software (version 4.0a, GraphPad Software, Inc., CA).

Size-exclusion chromatography (SEC) - PICUP reagents and phenolic compounds were removed from cross-linked samples by SEC as described previously(22). To do so, 1.5 cm diameter cylindrical columns were packed manually with 2 g of Bio-Gel P2 Fine (Bio-Rad Laboratories, CA), which produced a 6 ml column volume. The column first was washed twice with 25 ml of 50 mM NH_4HCO_3, pH 8.5. Two-hundred sixteen µl of cross-linked sample then was loaded. The column was eluted with the same buffer at a flow rate of ≈ 0.15 ml/min. The first 1 ml of eluate was collected. The fractionation range of the Bio-Gel P2 column is 100-1800 Da. Aβ peptides thus elute in the void volume whereas Ru(bpy) (MW=748.6), APS (MW=228.2), Myr (MW=318.2), RA (MW=360.3), and DTT (MW=154.2) enter the column matrix and are separated from Aβ.

Fractions were lyophilized immediately after collection. Reconstitution of the lyophilizates to a nominal concentration of 25 µM in 10 mM sodium phosphate, pH 7.4, followed by the SDS-PAGE analysis, showed that removal of reagents and phenolic compounds, lyophilization, and reconstitution did not alter the oligomer composition of any of the peptide populations under study (**Fig. S1**).

AFM - Peptide solutions were characterized using a Nanoscope IIIa controller (Veeco Digital Instruments, CA) with a multimode scanning probe microscope equipped with a JV scanner. All measurements were carried out in the tapping mode under ambient conditions using single-beam silicon cantilever probes. A 10 µl aliquot of each peptide lyophilizate, reconstituted to a concentration of 25 µM in 10 mM PBS, pH 7.4, was spotted onto freshly cleaved mica (Ted Pella, Inc., CA), incubated at room temperature for 5 min, rinsed with water, and then blown dry with air. At least four regions of the mica surface were examined to confirm the homogeneity of the structures throughout the sample. Mean particle heights were analyzed by averaging the measures values of eight individual cross-sectional line scans from each image only when the particle structure was confirmed.

NMR spectroscopy - Stock solutions of the five phenolic compounds (2.5 mM), and monomeric, uniformly ^{15}N-labelled Aβ42 peptide (0.25 mM) (rPeptide, GA) and Aβ40 (0.25 mM) were prepared by dissolution (with sonication) in aqueous basic solution (pD 11, 1 ml, 10 mM NaOD) (20). Aliquots of the Aβ42 and phenolic solutions were combined and mixed with cold (5°C) phosphate buffer solution (0.5-1.0 ml, 5 mM, pH 7.5) that contained 0.5 mM predeuterated ethylenediamine tetraacetic acid (Na_2EDTA-d_{12}), and 0.05 mM NaN_3. The aliquots were varied so that the final peptide:compound concentration ratio was 25 µM : 500 µM. To prevent aggregation, peptide solutions were kept cold (5°C) and standard ^1H-^{15}N HSQC spectra were obtained within 30-min of the sample preparation. Spectra were obtained at 5°C with a Bruker Avance-II 900 MHz spectrometer equipped with a TXI cryoprobe (Bruker BioSpin, Inc., CA).

The saturation transfer difference (STD) experiments were obtained with the Aβ40 (25 µM) alone or with RA or Myr (50 µM) at pH 7.5 and 5°C. Data was acquired at 900.18 MHz using the pulse program (selective irradiation)-(non selective excitation)-(watergate)-(acquisition) (23,24). The selective irradiation used a 3.9-s long and weak pulse that was alternatively applied at -0.2 ppm (where there was a peak) and at 30 ppm (where there was no peak), the latter constituting the reference spectra. The non-selective excitation was achieved with a 90° pulse at the water position (4.7 ppm), and the Watergate 3-9-19 pulse sequence was used to suppress the water signal. Each spectrum was acquired with 128-scans (12-min), and stored separately. The STD was obtained by subtracting the reference spectra from that obtained with irradiation at -0.2 ppm.

All NMR spectra were processed with the NMRPipe (25), Mnova (http://mestrelab.com/software/mnova-nmr/), or CARA (http://cara.nmr.ch) programs using a PC computer.

NMR-based molecular modeling - Atomic coordinates of the NMR/molecular dynamics Aβ42 structural model were kindly provided by Dr. Chunyu Wang (Rensselaer Polytechnic

Institute, NY) (26). With the model, the regions showing the most pronounced NH chemical shift movements (greater than 0.02 ppm) were revealed using the Swiss PDB Viewer program (27). These (backbone) regions were labeled with red color and the regions not showing movement with green color.

Cell culture - HEK 293 cells were cultured in 75-cm^2 flasks (Corning Inc., NY) in Dulbecco's modified Eagle's medium (DMEM)(Sigma-Aldrich, St. Louis, MO) containing 10% fetal bovine serum and incubated in a humidified chamber (85% humidity) containing 5% CO_2 at 37°C. One day before peptide sample treatment, the cell culture medium was replaced with serum-free DMEM, and the cells were trypsinized and re-plated onto coated 96-well plates at a final cell density of 20,000 cells/well.

Cytotoxicity assays - We used to test the toxicity of uncross-linked, cross-linked, cross-linked with Myr, and cross-linked with RA of Aβ42 as assessed in MTT assay. Peptide samples were prepared at Aβ concentrations of 2 μM and 20 μM in 10 mM sodium phosphate, pH 7.4. Aliquots of 50 μl were added to HEK cells to yield final Aβ concentrations of 1 and 10 μM. Twenty hours after the cells were incubated with peptide samples, MTT was added to each well, and the plates were kept in a CO_2 incubator for an additional 2 h. The cells were then lysed by adding lysis solution (50% dimethylformamide, 20% SDS at pH 4.7) and were incubated overnight. The degree of MTT reduction (i.e., cell viability) in each sample was subsequently assessed by measuring absorption at 590 nm at room temperature using a plate reader (PerkinElmer, Turku, Finland). Controls included medium with sodium phosphate ("negative") and 1 μM poly-L-lysine [ave. MW : 75000 Da] (Sigma-Aldrich) ("maximal positive"). Background absorbance values, as assessed from cell-free wells, were subtracted from the absorption values of each test sample. The absorbance measured from the three wells were averaged, and reported as mean ± S.E. percentage of cell viability

$$V = 100 - ((A_{A\beta} - A_{medium})/(A_{poly\text{-}L\text{-}lysine} - A_{medium})) \times 100$$

where $A_{A\beta}$, A_{medium}, and $A_{poly\text{-}L\text{-}lysine}$ were absorbance values from Aβ-containing samples, medium alone, or poly-L-lysine alone, respectively.

Electrophysiology - The fEPSPs were recorded from the CA1 region of acute hippocampal slices derived from C57BL/6 mice (male, 4-5 wk of age). The procedures for slice preparation and electrophysiological recording were described previously (28). Briefly, 300 μm thickness transverse hippocampal slices were placed in a physiological chamber perfused with artificial cerebrospinal fluid (ACSF; 125 mM NaCl, 3.5 mM KCl, 1.25 mM NaH_2PO_4, 25 mM $NaHCO_3$, 2.0 mM $MgSO_4$, 2.0 mM $CaCl_2$ and 20 mM glucose, aerated with a mixture of 95% O_2 and 5% CO_2) at a rate of 1 ml/min at 30°C. Shaffer collaterals/commissural bundle in the CA3 hippocampal subfield were stimulated using a bipolar stainless steel wire electrode at 20-sec intervals throughout the experiment. The fEPSPs were recorded from the stratum radiatum in the CA1 hippocampal subfield using a sharp glass electrode (2-6 MΩ, filled with 2 M NaCl). LTP was induced by tetanic stimulation delivered at 100 Hz for 1 sec. LTD was induced by low frequency 450 paired-pulse stimulation (50 msec paired-pulse interval, 1 Hz) for 7.5 min. LTD was induced only under the presence of cross-linked Aβ42 oligomer in this condition (see Results in detail). Each Aβ42 sample (500 nM in 0.3 mM NaOH in ACSF) or vehicle (0.3 mM NaOH in ACSF) was applied for 20 min so that Aβ42 sample/vehicle application overlapped and coterminated with conditioning stimulation for LTP or LTD. The evoked potential was amplified (x1000), filtered (0.1-1000 Hz), digitized (20 kHz) and stored in a computer for off-line analysis using PowerLab system (AD Instruments, Colorado Springs, CO). LTP and LTD values were presented as the percentage of average fEPSPs slope relative to the mean value of the baseline before conditioning stimulation.

Statistical analysis - One-way factorial ANOVA followed by Tukey-Kramer *post hoc* comparisons were used to determine statistical